Circadian regulation of endoplasmic reticulum calcium response in mouse cultured astrocytes

Ji Eun Ryu[1,2,†], Kyu-Won Shim[3,†], Hyun Woong Roh[1,4,†], Minsung Park[1,2], Jae-Hyung Lee[5*], and Eun Young Kim [1,2*]
[1]Neuroscience Graduate Program, Department of Biomedical Sciences, Ajou University Graduate School of Medicine, Suwon, Kyunggi-do 16499, Republic of Korea
[2]Department of Brain Science, Ajou University School of Medicine, Suwon, 16499, Kyunggi-do, Republic of Korea
[3]Interdisciplinary Program in Bioinformatics, Seoul National University, Seoul 08826, Republic of Korea,
[4]Department of Psychiatry, Ajou University School of Medicine, Suwon, 16499, Kyunggi-do, Republic of Korea
[5]Department of Oral Microbiology, College of Dentistry, Kyung Hee University, Seoul 02447, Republic of Korea
[†]These authors contributed equally.
*Correspondence: ekim@ajou.ac.kr(E.Y.K), Jae-Hyung Lee jaehlee@khu.ac.kr(J.L)

Abstract
The circadian clock, an internal time-keeping system orchestrates 24-hour rhythms in physiology and behavior by governing rhythmic transcription within cells. Astrocyte, the most abundant glial cell type, play crucial roles in central nervous system functions. However, a detailed understanding of how the circadian clock impacts functions of astrocyte remains largely unexplored. In this study, utilizing circadian clock-synchronized mouse cultured cortical astrocytes and RNA sequencing, we identified 412 circadian rhythmic transcripts with a distinct astrocyte-specific expression pattern. A Gene Ontology analysis of these rhythmic transcripts highlighted genes implicated in Ca^{2+} homeostasis as being under circadian control. Notably, Herpud1 (Herp) exhibited robust circadian rhythmicity at both mRNA and protein levels, a rhythm disrupted in astrocytes lacking the circadian transcription factor, BMAL1. HERP regulated endoplasmic reticulum (ER) Ca^{2+} release by modulating the degradation of inositol 1,4,5-trisphosphate receptors (ITPRs). Intriguingly, ATP-stimulated ER Ca^{2+} release varied with the circadian cycle, being more pronounced at subjective night, likely owing to the rhythmic expression of ITPR2. Furthermore, this rhythmic ER Ca^{2+} response led to day/night variations in the phosphorylation of Cx43 (Ser368) and the gap junctional communication. Given the role of gap junction channel (GJC) in propagating Ca^{2+} signals, we suggest that this circadian regulation of ER Ca^{2+} responses could markedly affect astrocytic modulation of synaptic activity according to the time of day. Overall, our study enhances the understanding of how circadian clock influences astrocyte function in the CNS, shedding light on their potential role in daily variations of brain activity and health.

Introduction
The circadian clock orchestrates a range of behaviors, physiological processes, and cellular and biochemical activities in organisms with approximately 24-hour rhythms, facilitating adaptation to environmental changes (Bell-Pedersen et al., 2005). In mammals, the master clock localized in the suprachiasmatic nucleus (SCN) of the anterior hypothalamus, synchronizes peripheral tissue clocks throughout the body to the light/dark cycle (Mohawk et al., 2012). The circadian clock's molecular mechanism is driven by a transcriptional translational feedback loop (TTFL). CLOCK and BMAL1 form a heterodimer that triggers expression of the repressor genes, *Period* (*Per*) and *Cryptochrome* (*Cry)*, in addition to other clock-controlled output genes. PER and CRY proteins then translocate to the nucleus, where they interact with CLOCK/BMAL1, halting further transcriptional activation. A secondary feedback loop involving the interplay between transcriptional activation by ROR and repression by REV-ERB finely regulates the rhythmic transcription of *Bmal1* (Takahashi, 2017). Recent studies have revealed that the circadian clock controls the rhythmic transcription of a large number of genes, displaying notable tissue specificity. This characteristic underscores the time-of-day-specific functional specialization of diverse tissues (Mure et al., 2018; Zhang et al., 2014). Consequently, circadian clock-controlled genes significantly influence various physiological processes including development, metabolism, aging, and neurodegeneration (Lananna & Musiek, 2020; Reinke & Asher, 2019; Schultz & Kay, 2003).
Astrocytes, a type of glial cell and the most abundant cell type in the CNS play vital roles in CNS function (Sofroniew & Vinters, 2010). They maintain the homeostasis of extracellular fluids, ions, and

neurotransmitters; provide energy substrates to neurons ; modulate local blood flow ; assist in interstitial fluid drainage . Beyond these roles, astrocytes interact functionally with brain cells including neurons and astrocytes, contributing actively to brain circuitry (Verkhratsky & Nedergaard, 2018). Though not electrically excitable, astrocytes exhibit complex intracellular Ca^{2+} signaling, both spatially and temporally, within individual astrocytes and across astrocytic networks, thereby influencing synaptic activity (Semyanov et al., 2020). Activation of Gq-protein coupled receptor (GPCR) by external stimuli initiates the inositol 1,4,5-trisphosphate receptor (IP_3R) signaling cascade, causing a release of Ca^{2+} from the ER that substantially increases intracellular Ca^{2+} levels (Guerra-Gomes et al., 2017; Verkhratsky & Nedergaard, 2018). Astrocytes express various types of Gq-coupled receptors activated by neurotransmitters such as ATP, epinephrine, glutamate, and dopamine etc. (Verkhratsky & Nedergaard, 2018). Increases in intracellular Ca^{2+} in astrocytes lead to alterations in cell-to-cell communication and/or induce gliotransmission (Giaume et al., 2021; Verkhratsky & Nedergaard, 2018). Recent studies have shown that astrocyte Ca^{2+} signaling can regulate organism-level behaviors, such as circadian rhythms and sleep patterns (Bojarskaite et al., 2020; Brancaccio et al., 2019) as well.

Accumulating evidence underscores the importance of the circadian clock in astrocytes function. First of all, cultured murine cortical astrocytes expressing a PER-luciferase reporter (PER::LUC) exhibit circadian oscillations per expression (Prolo et al., 2005). These astrocytes can be entrained by various cues, including temperature cycle (Prolo et al., 2005) and vasoactive intestinal polypeptide (VIP), which is the neuropeptide synchronizing SCN (Marpegan et al., 2009). These findings provide strong evidence that a molecular clock operates in astrocytes. In addition, disruption of clock genes specific to astrocytes has been linked to a range of deleterious effects, including excessive astrocyte activation, disruptions in daily activity patterns, impaired learning, metabolic imbalances, and a shortened lifespan (Barca-Mayo et al., 2020; Barca-Mayo et al., 2017; Griffin et al., 2019; Lananna et al., 2018). Remarkably, these phenotypic changes closely resemble those observed in astrocytes during the progression of neurodegenerative diseases (Brandebura et al., 2023; Phatnani & Maniatis, 2015). Moreover, the rhythmic metabolic activity of astrocytes, including intracellular Ca^{2+} fluctuations and neurotransmitter release, is critical for circadian timing in the SCN (Brancaccio et al., 2017). Despite the emerging significance of circadian rhythms in astrocyte function in health and disease, our understanding of the link between the circadian clock and specific astrocytic functions is still limited.

In this study, we conducted a transcriptome analysis to investigate how the circadian clock regulates astrocyte function. Our research uncovered that *Herp (*homocysteine-inducible ER protein with ubiquitin like domain 1; Herp) exhibited a BMAL1-dependent rhythmic expression pattern, peaking at midday and reaching its nadir at mid-night. Herp1 was important for ER Ca^{2+} regulation in cultured astrocytes. ATP stimulated ER Ca^{2+} response varied according to circadian time (CT), a dependence that was absent in cultured astrocytes from *Bmal1*$^{-/-}$ mice. This response was mediated by HERP1-mediated degradation of the inositol 1,4,5-triphosphate receptor 2 (ITPR2) degradation. Furthermore, the pronounced release of Ca^{2+} during the subjective night led to robust phosphorylation of the Ser368 residue of CONNEXIN 43 (CX43), likely diminishing cell-to-cell communication between astrocytes. Overall, our study demonstrates that the circadian clock orchestrates a variety of astrocytic processes including Ca^{2+} homeostasis by controlling the rhythmic transcription of genes, highlighting its pivotal role in CNS function.

Results

Defining circadian rhythmic transcripts in mouse cultured cortical astrocytes

To understand how the circadian clock regulates astrocyte physiology, we conducted a circadian transcriptome analysis in cultured mouse cortical astrocytes. Cultured astrocytes were subjected to serum shock (SS), which synchronizes the circadian clock, and then harvested at 4 hour intervals for 2 days beginning 12hrs after. A time series astrocyte transcriptome was determined RNA-seq (Fig. 1A). The Gaussian mixture model was used to define the sets of expressed transcripts. We chose 0.577 transcripts per million (TPM) as a cut-off, corresponding to the 1% threshold in the distribution curve of highly expressed genes (Fig. S1A). A total of 17,671 transcripts, with the highest value among the 12 time points exceeding the TPM threshold 0.577, were considered to be expressed. To validate astrocyte enrichment in our cell culture system, we compared the expression of marker genes for nervous cells (Fig. S1B). Time-merged mean TPM values indicated that transcriptome data were replete with astrocyte markers but lacked markers for microglia, oligodendrocytes, neurons, and endothelial cell.

To assess rhythmically oscillating genes in time-series transcriptome datasets, we applied BioCycle and MetaCycle packages, which have had been successfully used for this purpose (Agostinelli et al., 2016; Wu

et al., 2016), to the astrocyte transcriptome. BioCycle and MetaCycle analyses detected 321 and 311 periodic transcripts, respectively (FDR corrected, q-value < 0.05) (Fig. 1B). Among those transcripts, 220 (53.4%) were detected by both methods, but many transcripts were not overlapping. For example, *Plat* and *Il34* were detected as rhythmic only in BioCycle and *Mybph* and *Adora1* were detected rhythmic only in MetaCycle. Despite these incongruences, these four genes clearly exhibited a circadian rhythmic expression profile (Fig. S1C). Accordingly, we applied the union of two lists, identifying a total of 412 transcripts representing 2.3% of all transcripts as circadian rhythmic genes (Dataset S1). Oscillations of these 412 transcripts are illustrated in the heatmap in Fig. S1D.

Next, we compared rhythmic transcripts of astrocytes with those of 12 mouse tissues derived from CircaDB (Zhang et al., 2014), a database of genes that exhibit circadian expression patterns (Fig. S2A). Majority of rhythmic transcripts in astrocyte (265 of 412, 65.3%) was not rhythmic or rhythmic in one tissue. 14 transcripts were rhythmic in more than 10 tissues; most of these genes were core clock genes except *Tspan4*, *Tsc22d3*, *Wee1*. These results are consistent with previous reports that circadian rhythmic expression is controlled in a tissue specific manner (Mure et al., 2018; Panda et al., 2002). A comparison of the phases of these 14 common oscillating transcripts between CircaDB and our analysis showed that all 14 transcripts exhibited a consistent time difference between CircaDB and our analysis, where 8 hours after SS corresponded to CT0 (Fig. S2B). An additional comparison of phases of 82 transcripts that overlapped in only one tissue indicated a very robust phase correlation between astrocytes and the corresponding tissue ($r = 0.69$, $p < 0.001$) (Fig. S2C). Collectively, our analysis indicates that the identified oscillating transcripts were not false positive or noises but instead were clearly associated with the circadian clock. We then analyzed the phase distribution of oscillating transcripts by performing a hierarchical clustering analysis. For more intuitive and physiological interpretation, we transformed TASS phase in our data into CT phase by setting TASS 8 to CT0. Oscillating transcripts were divided into two clusters, with cluster 1 containing 185 transcripts and cluster 2 containing 227 transcripts (Fig. S3). A circular map of peak phases across all rhythmic genes revealed two major peaks; one early night peak (CT12 ~ CT16) and one late night or dawn peak (CT21 ~ CT1) (Fig. 1C). Circadian transcriptome studies conducted in multiple animal tissues have indicated that the phases of each tissue are not randomly distributed but are predominantly clustered in one or two narrow temporal windows (Panda et al., 2002). Consistent with these previous reports, mouse cultured astrocytes exhibited a high degree of temporal organization. Intriguingly, there was a relatively quiescent zone during subjective daytime, a finding different from that observed for diurnal animals, which showed a quiescent zone during subjective nighttime (Mure et al., 2018). To understand the biological processes and pathways controlled by the circadian clock, we performed a Gene Ontology (GO) analysis on each cluster using Metascape (https://metascape.org) (Fig. 1D). Given that the goal of our research was to investigate processes controlled by the circadian clock, we excluded 17 core clock transcripts-*Arntl, Clock, Nfil3, Npas2, Bhlhe40, Bhlhe41, Cry1, Cry2, Dbp, Elf, Nr1d1, Nr1d2, Per1, Per2, Per3, Rorc,* and *Tef* from our GO enrichment analysis. The analysis of the remaining transcripts showed that cluster 1, containing *Rhoc, Bcar1, Gpld1, Hspa5,* and *mmp14* etc. was enriched for the biological process “positive regulation of cell migration (GO:0030335). Time varying cell motility has been reported to be important for the circadian rhythms of wound-healing processes (Hoyle et al., 2017). Although astrocytes in the adult brain are largely non-motile under normal physiological conditions, their migratory activity is enhanced during the process of astrogliosis in the context of injury (Pekny & Pekna, 2016). Given this robust circadian rhythmic expression of genes that regulate motility, the expectation is that wound repair activity of astrocytes might vary according to the time of insult and would presumably be higher toward the end of the active period. Consistent with this, the biological processes, “regulation of cell-cell junction organization” and “cell-substrate adhesion” which are important for wound repair, were also enriched in the cluster 1. One of the biological processes enriched in cluster 2, was “calcium ion homeostasis (GO:0055074)” a term that was intriguing because of the importance of intracellular Ca^{2+} signaling in numerous astrocyte functions (Agulhon et al., 2008; Guerra-Gomes et al., 2017). Identified Ca^{2+} homeostasis-related genes included *Herp*, *Slc4a11*, *Sord* and *Kcnh1* etc. with *Herp* being the most significant gene with large oscillation amplitude (Table. S1).

Circadian rhythmic expression of *Herp* in mouse astrocyte culture

Herp was first identified as a novel gene that exhibited altered expression in response to homocysteine treatment in human umbilical vein endothelial cells (HUVECs) as part of a study on hyperhomocysteinemia (Kokame et al., 1996). Homocysteine induces ER stress and growth arrest in HUVECs (Outinen et al., 1999). Subsequent studies have shown that Herp is strongly induced not only by homocysteine but also by

drugs that cause ER stress, such as tunicamycin or thapsigargin. HERP, characterized by an N-terminal ubiquitin-like domain and present in the ER membrane, facing cytoplasmic side, has emerged as a novel target protein in the unfolded protein response (UPR) (Kokame et al., 2000). In particular, *Herp* is a member of the ER-associated degradation (ERAD) complex, which participates in ubiquitination and relocation of ERAD substrates, as demonstrated in several cell types (e.g. HEK 293T, MEF, NIH3T3 cells) (Leitman et al., 2014). Notably, a recent study reported that HERP is capable of modulating the ER Ca^{2+} response through IP_3R degradation (Paredes et al., 2016; Torrealba et al., 2017).
We first examined the expression patterns of core clock genes and *Herp* in our cultured astrocytes. *Bmal1*, the positive element of the TTFL, was rhythmically expressed with a peak at CT24. *Per2* and *Rev-Erb*α, clock genes downstream of CLOCK/BMAL1, were rhythmically expressed with peaks at CT12 and CT8, respectively (Fig. 2A). *Herp* showed a robust rhythmic expression pattern, with a peak at CT12, that was comparable to that of *Per2* (Fig. 2A). Then, in order to verify the circadian expression of *Herp*, we performed quantitative real-time RT-PCR (Fig. 2B). mRNA levels of *Bmal1*, *Rev-Erb*α and *Herp* exhibited circadian rhythm with similar phase of RNAseq results. Next, because many genes were rhythmically transcribed but their protein levels do not exhibit rhythmic changes (Reddy et al., 2006), we examined whether the levels of HERP were rhythmic. We first validated the specificity of HERP antiserum by performing Western blot analysis of astrocytes treated with siRNA targeting *Herp* (Fig. 2C - 2E). Herp siRNA greatly reduced both the levels of *Herp* mRNA (Fig. 2C) and the intensities of specific bands in Western blot analyses (Fig. 2D and 2E). Circadian clock synchronized cultured astrocytes were sampled every 6 hours for 2days and processed for Western blot analysis of BMAL1 and HERP. The phosphorylation status of BMAL1 exhibits circadian variation, such that hyper-phosphorylated BMAL1 peaks at midday and hypo-phosphorylated BMAL1 peaks early or at the end of the day (Yoshitane et al., 2009). In our SS-synchronized cultured astrocytes, BMAL1 was hyperphosphorylated at mid-day (e.g. CT10, 16, 34, and 40) and hypo-phosphorylated early or at the end of day (e.g. CT4, 22, 28, and 46) throughout two daily cycles (Fig. 2F) indicating the strong circadian rhythm of cultured astrocytes. Importantly, the levels of HERP proteins oscillated peaking at midday (CT10, CT34) and reaching a minimum early in the day or late at night (CT4, CT22, CT36), a pattern similar to that of its mRNA (Fig. 2F and 2G). Finally, to investigate whether the rhythmic expression of *Herp* is regulated by a circadian clock, we examined *Herp* mRNA and protein expression patterns in primary astrocyte cultured from *Bmal1*$^{-/-}$ mice. In *Bmal1*$^{-/-}$ astrocyte cultures, the rhythmic expression patterns of *Per2*, *Rev-Erb*α, and *Herp* were abrogated and their expression was maintained at trough levels (Fig. 2A). HERP protein levels were constant throughout the daily cycles (Fig. 2H and 2I). Collectively, these observations indicated that the expression of *Herp* exhibits a robust circadian rhythm that is controlled by BMAL1 in cultured mouse astrocytes. These results further suggest that HERP controlled cellular processes would vary according to CT.

Herp knockdown alters ATP-induced ER Ca^{2+} release

Next, we sought to investigate whether HERP-controlled processes are under circadian regulation. We examined HERP regulated ER Ca^{2+} response in the astrocytes, which have previously been reported in other cell types (Paredes et al., 2016; Torrealba et al., 2017) employing the organelle-specific fluorescent Ca^{2+} indicator G-CEPIA1er(Suzuki et al., 2014) (ER specific), R-GECO1(Wu et al., 2013) (cytosol specific), and mito-R-GECO1(Zhao et al., 2011) (mitochondria specific) . ATP serves not only as a fundamental energy source but also functions as an active intercellular messenger. In astrocytes, application of ATP induces an increase in intracellular Ca^{2+} (Neary et al., 1988), a process mediated by ATP binding to the G_q/G_{11} coupled P2Y receptor, which acts through activation of PLC-β and subsequent hydrolysis of PIP_2 to produce diacylglycerol (DAG) and IP_3, the latter of which then mobilize Ca^{2+} through IP_3Rs on the ER membrane (Baryshnikov et al., 2003; James & Butt, 2001). We treated control and *Herp* siRNA treated astrocytes with 100μM ATP and monitored subcellular changes in Ca^{2+}. ATP treatment rapidly decreased ER Ca^{2+} in control astrocytes and this response was greater in *Herp* siRNA treated astrocytes (Fig. 3A - 3C). The ER as the main Ca^{2+} store in the cell releasesCa^{2+} which is then rapidly transmitted to other organelles such as mitochondria and lysosomes and altered cytosolic Ca^{2+} signals. Although ATP treatment did not significantly alter cytosolic Ca^{2+} signal in control astrocytes, it greatly increased cytosolic Ca^{2+} signals in *Herp*-knockdown astrocytes (Fig. 3D – 3F). Consistently, mitochondrial Ca^{2+} was greatly increased under *Herp* siRNA condition compared with control (Fig. 3G – 3I). These results indicated that HERP controls ER Ca^{2+} responses in astrocytes thereby impacting diverse subcellular signaling processes.

Next, we examined the mechanism by which HERP controls ER Ca^{2+}.There are three subtypes of IP_3Rs encoded by the genes *Itpr1*, *Itpr2*, and *Itpr3*. In our cultured astrocytes, transcriptome analysis indicated *Itpr1* as the most prevalent, followed by *Itpr2*, while *Itpr3* expression was minimal (Fig. S4). Notably, expression of *Itpr* subtypes was not rhythmic. We then assessed the ITPR1 and ITPR2 protein levels in control and *Herp*-knockdown astrocytes and found that the levels of both ITPR1 and ITPR2 were slightly but statistically significantly increased in in *Herp* siRNA-treated astrocytes compared with controls (Fig. 3J – 3M). This suggests that HERP regulates ER Ca^{2+} release via IP_3R degradation in astrocytes.

ATP-induced ER Ca^{2+} release varies according to CT

Because the amount of HERP exhibited circadian variation and HERP regulates ER Ca^{2+} release, we next investigated whether ATP-induced ER Ca^{2+} responses differ different depending on CT. After synchronizing cultured astrocytes, we measured ER Ca^{2+} following ATP treatment at peak (CT34) and trough (CT22) HERP time points (Fig. 4A). Because the levels of HERP were lower at CT22 resulting in higher IP_3R levels it is conceivable that ER Ca^{2+} release might be greater at CT22 than at CT34. Consistent with this, ER Ca^{2+} decreased to a greater extent at CT22 than at CT34 upon ATP treatment (Fig. 4B – 4D). Also, in keeping with this prediction, cytosolic Ca^{2+} increased to a greater extent at CT22 than at CT34 following ATP treatment (Fig. 4E - 4G). Although variations in mitochondrial Ca^{2+} responses exhibited a consistent circadian tendency as well, but this trend did not reach statistical significance (Fig. 4H – 4J). Finally, we assessed whether the levels of ITPR1 and ITPR2 varied according to CT. The phosphorylation status of BMAL1 served as a proxy for CT (Fig. 4K). The levels of ITPR2 showed CT-dependent changes opposite those of HERP, whereas ITPR1 levels were constant at both CTs (Fig. 4K and 4L). Because *Itpr2* mRNA levels did not show a rhythmic pattern (Fig. S4), we reasoned that the CT-dependent differences in ITPR2 levels were mainly driven by HERP-mediated ITPR2 degradation. The fact that ITPR1 levels were constant further support the conclusion that circadian rhythmic ER Ca^{2+} responses are mainly driven by oscillations in ITPR2.

Finally, we sought to confirm that ATP-induced ER Ca^{2+} response is controlled by the circadian clock by analyzing this response in cultured astrocytes from *Bmal1*$^{-/-}$ mice. This analysis showed no CT differences in the decrease in ER Ca^{2+} following ATP treatment (Fig. 5A – 5C). The absence of rhythmic ER Ca^{2+} responses in Bmal1$^{-/-}$ astrocytes was associated with unchanging levels of HERP (Fig. 5D - 5E). We also noticed that the ER Ca^{2+} decrease was greater in Bmal1$^{-/-}$ astrocytes than in control astrocytes (Fig. 4D and 5C), a difference that might be explained by the fact that HERP levels in Bmal1$^{-/-}$ astrocytes were comparable to trough levels observed in control astrocytes (Fig. 5E). Collectively, these results clearly indicate that the circadian clock controls rhythmic ER Ca^{2+} responses through rhythmic oscillations in HERP levels in cultured mouse astrocytes.

ATP-induced S368-phosphorylation of Cx43 and gap junctional communication shows circadian variation.

Syncytial coupling achieved through gap junctions is the prominent feature of astrocytes. This coupling is critical for the homeostatic function of astrocytes through enhancing diffusion and equilibration of ions, metabolites, and signaling molecules (Langer et al., 2012; Verkhratsky & Nedergaard, 2018). In addition, the astrocytic syncytium can propagate Ca^{2+} waves that affect nearby and remote cells through release of “gliotransmitters”, by which astrocytes can modulate synaptic functions in a far-reaching network (Pacholko et al., 2020). Connexin (Cx) family proteins are the molecular constituents of gap junction channels (GJCs) (Giaume et al., 2021). Cx43 (also known as Gja1) and Cx30 (also known as Gjb6) are the main connexins of astrocytes (Kunzelmann et al., 1999; Nagy et al., 1999). In our cultured astrocytes, the most abundantly expressed connexin was Cx43 (Fig. S5). The phosphorylation of Cx43 at Ser368 by protein kinase C (PKC), activated in response to intracellular Ca^{2+}, is known to decrease gap junction conductance (Enkvist & McCarthy, 1992; Nimlamool et al., 2015; Solan & Lampe, 2014). Accordingly, we reasoned that the circadian variation in ATP-driven ER Ca^{2+} responses might differentially impact Cx43 phosphorylation according to times of day. We first confirmed that treatment of cultured astrocytes with ATP induced rapid phosphorylation of Cx43 at Ser368 (Fig. 6A and 6B). We then examined whether phosphorylation of Cx43 at Ser368 varied depending on CT. Notably, ATP-induced ER Ca^{2+} release was more pronounced at CT22 than at CT34 (Fig. 3). The phosphorylation of Cx43 at Ser368 in response to ATP treatment, was also significantly higher at CT22 compared with that at CT34 (Fig. 6C and 6D).

Next, we examined whether circadian variations in Cx43 phosphorylation occurred *in vivo*. To this end, we entrained mice to a 12:12 hour light/dark (LD) cycle for two weeks and then maintained them in constant

darkness (DD). Probing samples under constant darkness ensured that variations in Cx43 phosphorylation were due to the internal circadian clock and not external light stimuli. Prefrontal cortex tissues were dissected at CT58 and CT70 at third days of DD and Ser368-phosphorylated Cx43 (pCx43) was measured. Intriguingly, Cx43 phosphorylation was pronounced at subjective night, consistent with our *in vitro* results. Finally, we sought to assess whether gap junctional communication shows CT variation in cultured astrocytes by utilizing the fluorescence recovery after photobleaching (FRAP) method. Initially, we confirmed the role of gap junctions in intercellular communication in cultured astrocytes by observing the absence of fluorescent signal recovery after applying the gap junction channel blocker, carbenoxolone (CBX) (Fig. S6A – S6C), which was in line with previous studies (Santiquet et al., 2012). Subsequently, we investigated CT dependent variations in this communication. We observed a more rapid and pronounced recovery of fluorescence in photobleached astrocytes during subjective day (e.g., CT34) compared with subjective night (e.g., CT22) (Fig. 6G – 6I). Interestingly, this variation was absent in astrocytes cultured from Bmal1$^{-/-}$ mice, indicating that the day and night variations in gap junctional communication is regulated by circadian clock (Fig. 6J. – 6L).

In summary, we provide a model illustrating how circadian clock influences astrocyte function through the regulation of ER Ca^{2+} response. In astrocytes, the BMAL1/CLOCK-controlled oscillation of HERP regulates day and night variations in ITPR2 levels. These oscillations contribute to changes in ER Ca^{2+} responses, which in turn associate with distinct differences between day and night in the phosphorylation of Cx43 at Ser368 and the conductance of the gap junction channel (GJC).

Discussion

It is widely acknowledged that the circadian clock orchestrates cellular functions in a highly cell type-specific manner by governing transcription (Mure et al., 2018; Zhang et al., 2014). Although there is ample evidence attesting to the importance of the circadian clock in astrocytes (Barca-Mayo et al., 2020; Barca-Mayo et al., 2017; Griffin et al., 2019; Lananna et al., 2018; Prolo et al., 2005; Tso et al., 2017), explorations of how the circadian clock precisely modulates astrocytic functions employing astrocyte-specific circadian transcriptome analyses have been limited. Our study conducted such an analysis on primary cultured cortical astrocytes and discovered that rhythmic expression of *Herp* underlies day/night variation in ER Ca^{2+} response, showing that HERP acts by altering IP_3R levels. We also found that Ca^{2+}-activated Cx43 phosphorylation varied in accordance with the daily rhythmic ER Ca^{2+} response. Given that astrocytes function in a network in which Ca^{2+} propagates through GJCs, we propose that the time-dependent control of ER Ca^{2+} responses could influence the synaptic activity modulating role of astrocytes (see below).

In this study, we discovered that 2.3 % of all transcripts showed circadian rhythmic expression with astrocyte specificity. Notably, numerous genes associated with key astrocyte functions such as “regulation of systemic arterial blood pressure”, “cell migration”, “metabolic processes”, “G protein coupled receptor signaling”, and “ion transport” etc. appeared to be controlled by the circadian clock. Of particular interest, *Herp* exhibited rhythmic expression in phase with *Per2* in primary cultured astrocytes. In *Bmal1*$^{-/-}$ astrocyte cultures, *Herp* showed flattened expression at its nadir level, suggesting that its transcription is directly regulated by CLOCK/BMAL1 heterodimers (Fig. 2A). Although no canonical E box was found in the upstream 6 Kb region of the *Herp* gene , a previous ChIP-Atlas analysis (https://chip-atlas.org)(Oki et al., 2018; Zou et al., 2022) demonstrated CLOCK binding to the *Herp* genomic region (Annayev et al., 2014; Hong et al., 2018). Additionally, the TTFL repressors E4BP4 (Adenovirus E4 promoter Binding Protein 4), also referred to as NFIL3 (Nuclear Factor Interleukin 3), as well as the activators TEF (Thyrotroph Embryonic Factor) and HLF (Hepatic Leukemia Factor) also bind to the *Herp* genomic region (Dunham et al., 2012; Liu et al., 2022; Yoshitane et al., 2019). Oscillations in *Herp* expression have been previously documented in various mouse tissues including the lung, heart, liver, kidney, aorta, skeletal muscle, adrenal gland, pancreatic islet and SCN (Panda et al., 2002; Rakshit et al., 2016; Zhang et al., 2014). Collectively, this wealth of evidence strongly suggests that *Herp* is subject to direct regulation by the circadian clock. Our study further demonstrated that *Herp* oscillates at both mRNA and protein levels in cultured astrocytes. The significance of HERP in modulating circadian variations in Ca^{2+} signaling in the afore-mentioned tissues and cells is an intriguing avenue for future research. Interestingly, a recent study employing a circadian single-cell RNA seq analysis of SCN reported that *Herp* displays a circadian rhythm exclusively in astrocytes and oligodendrocytes (Wen et al., 2020). Given that astrocytic Ca^{2+} levels in the SCN demonstrated a circadian rhythm, peaking during the subjective night and are crucial for circadian timing (Brancaccio et al., 2019; Patton et al., 2022), HERP’s circadian rhythmic expression in SCN astrocytes (Wen et al., 2020) may be integral to the mechanisms of circadian timing.

We demonstrated that HERP regulated ER Ca^{2+} responses by degrading IP_3Rs in astrocytes, aligning with findings in other cell types (Fig. 3J – 3M). (Paredes et al., 2016; Torrealba et al., 2017). There are three subtypes of IP_3Rs in astrocytes encoded by the genes *Itpr1*, *Itpr2*, and *Itpr3.* While all three subtypes are expressed in our cultured astrocytes, *Itpr3* was expressed in negligible amounts (Fig. S4). Traditionally, ITPR2 has been regarded as a major subtype closely associated with astrocyte function (Holtzclaw et al., 2002; Sharp et al., 1999) and accumulating evidence has shown that not only ITPR2, but also ITPR1 and ITPR3 are important in astrocyte Ca^{2+} signaling, with each subtype eliciting distinct Ca^{2+} responses (Sherwood et al., 2021). When *Herp* was downregulated, the levels of both ITPR1 and ITPR2 increased, but only the levels of ITPR2 exhibited day/night variation (Fig. 3J – 3M, Fig. 4K – 4L). The min/max ratio of HERP expression throughout the day was 0.38 under normal conditions, but was 0.072 in *Herp*-KD conditions. Based on our study, we reasoned that the amplitude of HERP oscillations impacted the levels of ITPR2 under normal circumstances, while having a much lesser effect on the levels of ITPR1. Thus, we conclude that the circadian control of ER Ca^{2+} release in response to stimulation in cultured astrocytes is attributable to ITPR2.

Our study revealed distinct circadian variations in ER and cytosolic Ca^{2+} responses following ATP treatment that were not reflected in mitochondrial Ca^{2+} responses (Fig. 4). Upon ATP stimulation, Ca^{2+} is released from the ER via IP_3R, and subsequently enters both the cytosol and mitochondria. In the cytosol, direct Ca^{2+} transfer occurs through IP_3R. For mitochondrial uptake, Ca^{2+} first transits to the intermembrane space via IP_3Rs and the voltage-dependent anion channel (VDAC) complex before entering the matrix through mitochondrial calcium uniporter (MCU) (Giorgi et al., 2018). The Mito-R-GECO1 reporter used in our studies of changes in mitochondrial Ca^{2+} is confined within the mitochondrial matrix and thus cannot assess Ca^{2+} levels in in the intermembrane space (Wu et al., 2013). Thus, we think of several possibilities to account for the absence of significant circadian variations in mitochondrial Ca^{2+} in response to ATP stimulation relative to cytoplasmic Ca^{2+} change. First, substantial changes in Ca^{2+} levels might occur in the intermembrane space, but the influx into the matrix via MCUs could remain constant across different CT, resulting in apparent lack of significant change. Second, the amount of VDAC or the VDAC:IP3R complex on the mitochondrial membrane might vary inversely with HERP levels, potentially maintaining a consistent flow of Ca^{2+} into the mitochondria irrespective of the CT. Additionally, the presence of several Ca^{2+} extrusion mechanisms in mitochondria (Giorgi et al., 2018) points to a more complex regulation of Ca^{2+} compared with that in the cytosol. Although the precise mechanism remains to be elucidated, our data indicate that the circadian variation in Ca^{2+} release from the ER, particularly in response to stimuli, predominantly impacts cytoplasmic signaling rather than mitochondrial signaling.

Importantly, we discovered that during the subjective night (active period for mice), ATP- stimulated ER Ca^{2+} release was pronounced compared with that during the subjective day (rest period for mice) (Fig. 4). This finding aligns with recent studies that emphasized the role of astrocytic Ca^{2+} in sleep regulation. In mice, stimulus-evoked Ca^{2+} activity in astrocytes was found to be heightened during wakefulness and diminished as sleep progressed (Bojarskaite et al., 2020; Ingiosi et al., 2020). In flies, Ca^{2+} activity in astrocytes is correlated with the duration of wakefulness, suggesting that astrocytic Ca^{2+} is a key factor in the homeostatic regulation of sleep (Blum et al., 2021). Collectively, these reports collectively underscore the role of astrocytic Ca^{2+} signaling in sleep homeostasis. Our observations that ATP-stimulated ER Ca^{2+} release is elevated during the subjective night compared with the subjective day provides a mechanistic explanation for the differential Ca^{2+} levels observed between wake and sleep states. Notably, the circadian regulation of ITPR2 by HERP might be a fundamental factor in this process.

We also observed a marked increase in ATP-stimulated Cx43 (S368) phosphorylation during the subjective night compared with the subjective day (Fig. 6C and 6D.). This observation was further supported by in *vivo* experiments, which demonstrated higher levels of pCx43(S368) in the frontal cortex during the subjective night than during the day (Fig. 6E and 6F). What are the implications of this day/night variation in Cx43 (S368) phosphorylation? Cx43 and Cx30 are the main connexins in astrocytes, where they constitute key components of gap junctions (Kunzelmann et al., 1999; Nagy et al., 1999). Gap junctions mediate intercellular communication by providing ultrastructural cytoplasmic continuity and are thus integral to formation of the functional syncytium of astrocytes (Giaume et al., 2010; Kiyoshi & Zhou, 2019). In our study, Cx43 was the main connexin and was most abundantly expressed, whereas Cx30 expression was almost negligible (Fig. S5). Cx43 possesses a distinctive structural composition consisting of an extensive C-terminal tail, an N-terminal domain, and multiple transmembrane segments. The C-terminal tail contains sites for post-translational modifications. Specifically, Cx43 has more than 10 phosphorylation sites, and its phosphorylation is key to the control of its function (Pogoda et al., 2016; Solan & Lampe, 2014). Among

these sites Ser368 is a target for phosphorylation by PKC, which becomes activated in response to elevated Ca^{2+} levels; notably this phosphorylation event leads to the closure of Cx43 gap junction channels (Enkvist & McCarthy, 1992; Nimlamool et al., 2015; Pogoda et al., 2016; Pun et al., 2022; Solan & Lampe, 2014, 2016). We reasoned that the circadian variation in Cx43 phosphorylation could be significant in terms of astrocyte functionality within the syncytium. Indeed, in our cultured astrocytes, gap junctional communication exhibited day and night variation (Fig.6G – 6I). Astrocytes influence synaptic activity through the release of gliotransmitters such as glutamate, GABA, D-serine, and ATP, triggered by increases in intracellular Ca^{2+} in response to the activity of adjacent neurons and astrocytes (Verkhratsky & Nedergaard, 2018). Importantly, this increase in Ca^{2+} spreads to adjacent astrocytes through GJCs (Fujii et al., 2017), influencing a large area of the neuronal network. Considering that Cx43 Ser368 phosphorylation occurs to uncouple specific pathways in the astrocytic syncytium to focus local responses (Enkvist & McCarthy, 1992), our findings suggest that astrocytes better equipped for localized responses when presented with a stimulus during the active phase in mice. Conversely, during the rest period, characterized by more synchronous neuronal activity across broad brain areas (Vyazovskiy et al., 2009) higher GJC conductance might allow astrocytes to exert control over a larger area. In support of this idea, recent study showed that synchronized astrocytic Ca^{2+} activity advances the slow wave activity (SWA) of the brain, a key feature of non-REM sleep (Szabó et al., 2017). Blocking GJC was found to reduce SWA, further supporting this interpretation. However, conflicting findings have also been reported. For instance, Ingiosi et al. (Ingiosi et al., 2020) found that astrocytic synchrony was higher during wakefulness than sleep in the mouse frontal cortex. Whether these differing results in astrocyte synchrony during resting and active periods are attributable to differences in experimental context (e.g., brain regions, sleep-inducing condition) remains unclear. Indeed, astrocyte Ca^{2+} dynamics during wakefulness/sleep vary according to brain regions (Tsunematsu et al., 2021). While the extent of astrocyte synchrony might differ depending on brain region and/or stimulus, on our results suggest the conclusion that that the baseline state of astrocyte synchrony, which is affected by GJC conductance, varies with the day/night cycle.

The presence of various glial subpopulations, each with high expression of multiple connexins, contributes to the formation of a "panglial syncytium." This allows gap junction channels to form between astrocytes and other glial or non-glial cells (Fróes et al., 1999; Rash et al., 1997). Astrocytic GJCs connecting both oligodendrocytes and ependymal cells lining the ventricles have been reported (Rash et al., 1997). Recent studies in mice with cell type-specific deletion of connexins have demonstrated that removal of the astrocytic connexins (Cx30 and Cx47) results in the total disruption of panglial coupling. Moreover, this coupling can be maintained if at least one allele of either connexin is retained (Griemsmann et al., 2015). Based on our experimental findings, we conclude that phosphorylation of Cx43 at Ser368 in response to a stimulus is contingent on CT and consequently influences the permeability of GJCs in a CT dependent manner. Drawing from previous research, this could have substantial implications not only for GJs between astrocytes, but also for those linking astrocytes with other cell types, such as oligodendrocytes, and other cell types.

In conclusion, our findings significantly enhance the understanding of the circadian regulation of astrocytic functions, particularly through the rhythmic expression of HERP and its impact on ER Ca^{2+} signaling and Cx43 phosphorylation. This study underscores the intricate interplay between the circadian clock and astrocyte physiology, highlighting the pivotal role of HERP in modulating key astrocytic processes such as sleep, gap junction communication and synaptic modulation. The day/night variations in ER Ca^{2+} response and Cx43 phosphorylation, and their implications for astrocytic network dynamics and neuronal interactions, open new avenues for exploring the broader implications of astrocytic circadian rhythms in brain function and health. Thus, this work not only contributes to our fundamental understanding of astrocyte biology, it also has potential implications for addressing neurological disorders where circadian and astrocytic dysfunctions intersect.

Materials and Methods

Animals

All procedures for the care and use of laboratory animals were approved by the Institutional Animal Care and Use Committee (IACUC) of Ajou University School of medicine. Initially, Bmal1$^{-/+}$ mice (B6.129-Bmal1^{tm1Bra}/J; Jackson Laboratory), #009100)(Bunger et al., 2000) were purchased from Jackson Laboratory(USA) and housed in a specific pathogen-free environment at the Animal Research Center of Ajou University Medical Center, with a standard 12-hour light/dark cycle and free access to food. In

experiments employing primary cultured astrocytes from Bmal1$^{-/-}$ mice, wild type (WT) littermates were used as controls. Primary cultured astrocytes involving only WT mice used 1 day-old C57BL/6 mice (Koatch Inc., Korea) For animal studies, 7-8 week-old adult C57BL/6 male mice were first entrained in a standard 12-hour light/dark cycle for 2 weeks and then maintained in a constant darkness (DD). On the third day of DD, mice were sacrificed at indicated circadian time (CT) and its prefrontal cortex (PFC) was dissected.

Primary astrocyte culture

Cultures of primary astrocytes were prepared according to a previous report (Choi et al., 2018) with minor modifications. In brief, 1 day old pups were anesthetized by hypothermia and their cerebral cortices were dissected out and triturated in Modified Eagle's medium (MEM; Welgene(Korea), LM 007-11) containing 10% fetal bovine serum (FBS; Hyclone(USA), SV30207.02), penicillin/streptomycin (Gibco(USA), 15140-122), 10 μM HEPES (Gibco, 15630080) and GlutaMAX (Gibco, 35050-061) yielding a single-cell suspension. Cells were plated into 75 cm^2 T-flasks (1pup/flask) and incubated at 37°C in a humidified 5% CO_2 incubator for 2 weeks. Primary astrocytes were then incubated in serum-free MEM for 7 days, after which astrocytes were detached from the T-flask with 0.25% trypsin and plated on culture dishes ($1.0X10^6$cells/60 mm dish) for further experiments.

Circadian transcriptome analysis

The experimental scheme for synchronizing circadian clocks of cultured astrocyte is depicted in Figure 1A. In brief, astrocytes were grown in dishes (1.0 X 10^6cells/60 mm dish) until reaching complete confluence and then incubated in serum-free MEM for 72 hours. Cells were then subjected to serum shock (SS), a well-established procedure for synchronizing the circadian clock of cultured cells (Balsalobre et al., 1998), by exchanging the medium for MEM containing 50% horse serum. Twelve hours after SS, astrocytes were harvested at 4-hour intervals for 2 days for RNA sequencing (RNA-seq).

Total RNA was extracted and purified from harvested astrocytes using an RNeasy Plus Micro Kit (Qiagen (Germany), 74034). RNA quality and quantity assessments, RNA-Seq library construction, and next-generation sequencing analysis were performed by Macrogen Inc. (Korea). Total RNA integrity and library size were analyzed using an Agilent Technologies 2100 Bioanalyzer. Paired-end raw reads, generated using an Illumina HiSeq 2000 system, were aligned to the mm10 mouse genome using STAR aligner (v.2.5.2b)(Dobin et al., 2013). Gene expression was subsequently quantified by calculating transcripts per million (TPM) using Ensemble gene (release 82) annotations. The threshold for defining expressed transcripts was set using a Gaussian mixture model in the R package 'mixtools'

To detect circadian oscillating transcripts, we employed two circadian oscillation detection methods BioCycle(Agostinelli et al., 2016) and MetaCycle (Wu et al., 2016). BioCycle contains various types of oscillating signal patterns, and deep learning methods was applied to develop and train algorithms. MetaCycle incorporates ARSER, JTK_CYCLE, and Lomb-Scargle algorithm for period signal detection (Wu et al., 2016). We tested both methods and decided to use union of rhythmic transcript lists from two methods. For the biological and functional annotations for the identified circadian clock transcripts, we used Metascape (https://metascape.org)(Zhou et al., 2019) with default express analysis option.

Quantitative reverse transcription polymerase chain reaction (qRT-PCR)

Total RNA was extracted from cells and purified using the RNeasy Plus Micro Kit (Qiagen ,74034). 1μg of total RNA was reverse transcribed using an oligo-dT primer and PrimeScript RTase (TaKaRa (Japan), 2680A). Quantitative real-time PCR was performed using a Rotor Gene Q (Qiagen) with TB Green Premix Ex Taq (Takara, RR420A) The specific primers used were provided in the Supplementary Table 1. Noncycling mRNA encoding HPRT was used to normalize gene expression. The data were analyzed

using Rotor Gene 6000 software, and the relative mRNA levels were quantified using the 2-2-ΔΔCt method in which ΔΔCt=[(Ct target – Ct HPRT) of experimental group] – [(Ct target – Ct HPRT) of control group].

siRNA transfection and Immunoblotting

The following On-Target plus SMARTpool siRNAs were purchased from Dharmacon (USA) : Non-targeting control siRNA(D-001810-01-50), Herp siRNA (L-049714-01-0005), Itpr1 siRNA(L-040933-00-0005), and Itpr2 siRNA(L- 041018-00-0005). After cells had reached greater than 90% confluence, the medium was changed to serum-free MEM and cells were incubated for 72 hours. Cells were then transfected with siRNA using Lipofectamine RNAiMAX (ThermoFisher (USA), 13778150) according to manufacturer's protocol. Experiments were performed 48 hours after transfection.

For immunoblotting, astrocytes were lysed using modified-RIPA buffer (50 mM Tris-HCl pH 7.4, 1% NP-40, 0.5% sodium deoxycholate, 150 mM NaCl) supplemented with protease inhibitor cocktail (Sigma-Aldrich (USA), P8340) and phosphatase inhibitor cocktails 2 and 3 (Sigma-Aldrich, P5726 and P0044). Proteins were separated by sodium dodecyl sulfate-polyacrylamide gel electrophoresis (SDS-PAGE) and transferred to polyvinylidene fluoride membranes. After blocking with 5% skim milk, membranes were incubated overnight at 4°C with the following primary antibodies at the indicated dilutions: anti-BMAL1 (Abcam (UK), ab93806), 1:2000; anti-HERP (Abcam, ab150424), 1:1000; anti-ITPR1 (Abcam, ab264284), 1:1000; anti-ITPR2 (Alomone Labs (Israel), ACC-116),1:1000; anti-Cx43 (Sigma, C6219), 1:5000; anti-pCx43 (Ser368) (CST (USA), 3511), 1:1000; anti-GAPDH (Novus (USA), NB100-56875), 1:5000; anti-vinculin (Sigma-Aldrich, V4505), 1:5000; and anti-total ERK (CST, 9102), 1:5000. Membranes were washed with Tris-buffered saline containing 0.5% Tween 20 (TBST), incubated with secondary antibodies, and visualized using an enhanced chemiluminescence system. Protein levels were quantified densitometrically by measuring band intensities using Image J software.

Ca2+ reporter plasmid transfection and imaging analysis

After cells reach greater than 90% confluence, the medium was changed to serum free MEM. Ca^{2+} measurement was conducted using pCMV-G-CEPIA1er, a gift from Masamitsu Iino (Addgene (USA) plasmid #58215)(Suzuki et al., 2014), and CMV-R-GECO1 and CMV-mito-R-GECO1, gifts from Robert Campbell (Addgene plasmids #32444, #46021)(Wu et al., 2013; Zhao et al., 2011). These plasmids, encoding Ca^{2+} indicators, were transfected into cells 72 hours after switching to serum-free conditions, with or without siRNA, using Lipofectamine 2000 according to manufacturer's protocol. Forty-eight hours after transfection, the medium was replaced with Hanks balanced salt solution (HBSS) without Ca^{2+} and Mg^{2+} (Gibco, 14175095), and fluorescence images were acquired every 3 seconds using a Nikon A1R Confocal Microscope system equipped with a x60 1.4 NA Plan-Apochromat objective (Nikon Instrument, Inc. (Japan)) at 37°C in a humidified 5% CO_2 atmosphere. These experiments were performed at the Three-Dimensional Immune System Imaging Core Facility of Ajou University (Korea). Images were analyzed using an NIS elements C program. Fluorescence intensity was measured at each time point (F_t) and ΔF values were calculated from (F_t – F_0). F_0 values, used for normalization, were defined by averaging 10 frames before stimulation.

Gap-FRAP (fluorescence recovery after photobleaching) analysis

Astrocyte communication was assessed using the gap-FRAP assay with slight modifications from a previous report (Santiquet et al., 2012). This involved quantifying the transfer of the fluorescent dye calcein from cells to another cell that had been subjected to laser bleaching to remove calcein fluorescence. Thirty minutes prior to imaging, cells were loaded with 0.5uM Calcein-AM (Invitrogen (USA), C1430) and 0.05% Pluronic-127 (Invitrogen, P6866) at 37°C. A 30min incubation period allowed for the dye to diffused and be cleaved into fluorescent calcein, after which cells were rinsed twice with serum free MEM. In experiments involving CBX treatment, CBX (20μM) was applied for an additional 30 minutes after calcein incubation. Immediately before imaging, the medium was switched to HBSS without Ca^{2+} and Mg^{2+} (Gibco, 14175095). Utilizing a Nikon A1R Confocal Microscope system equipped with a 488nm argon laser and a x60 1.4 NA

Plan-Apochromat objective (Nikon Instruments, Inc.), photobleaching was performed on ROI cell, and fluorescence was measured under 37°C in a humidified atmosphere of 5% CO2. Fluorescence intensity was captured in a confocal plane during the following intervals: five pre-bleach images, a 15-second 100% power laser pulse at a stimulation speed of 5.3 lines/sec in the ROI cell, and an image taken every 3 seconds for a 3-minute post-bleach period. Images were analyzed using NIS elements C program. Fluorescence intensity was measured at each time point (F_t) and normalized intensity values were calculated as F_t/F_0. F_0 values, used for normalization, were defined by averaging 5 frames before bleaching. Recovery % calculated as $(F_{FR}-F_A)/(F_0-F_A)x100$, where F_{FR} is full recovery fluorescence intensity after photobleaching and F_A is the fluorescence intensity right after photobleaching.

QUANTIFICATION AND STATISTICAL ANALYSIS

Statistical analyses were performed using GraphPad Prism 8 software. Differences between two groups were analyzed using independent t-tests. Differences among three or more groups were analyzed by one-way analysis of variance (ANOVA) with Tukey's post hoc test. A repeated measures two-way ANOVA was employed for comparison of multiple groups and conditions. Differences were considered significant for p-values < 0.05.

Data and code availability

- Circadian RNA sequencing data have been deposited at GEO under accession number GEO: GSE254678.
- Any additional information required to reanalyze the data reported in this paper is available from the E.Y.K upon request.

Acknowledgments

We are very grateful to Eunhye Joe and all members of Eun Young Kim's laboratory for critical comments on the manuscript. This research was supported by National Research Foundation of Korea (NRF) grants funded by the Korean government (Ministry of Science and ICT; grant numbers, 2019M3C7A1031905, 2019R1A5A2026045).

Author Contributions

J.E.R., H.W.R., J.L., and E.Y.K designed research. J.E.R., K. S., H.W.R., and J.L. performed research. All authors analyzed data. J.E.R. and E.Y.K. wrote the first draft of the manuscript and all authors contributed to revising the manuscript.

Declaration of interests

The authors declare no competing interests.

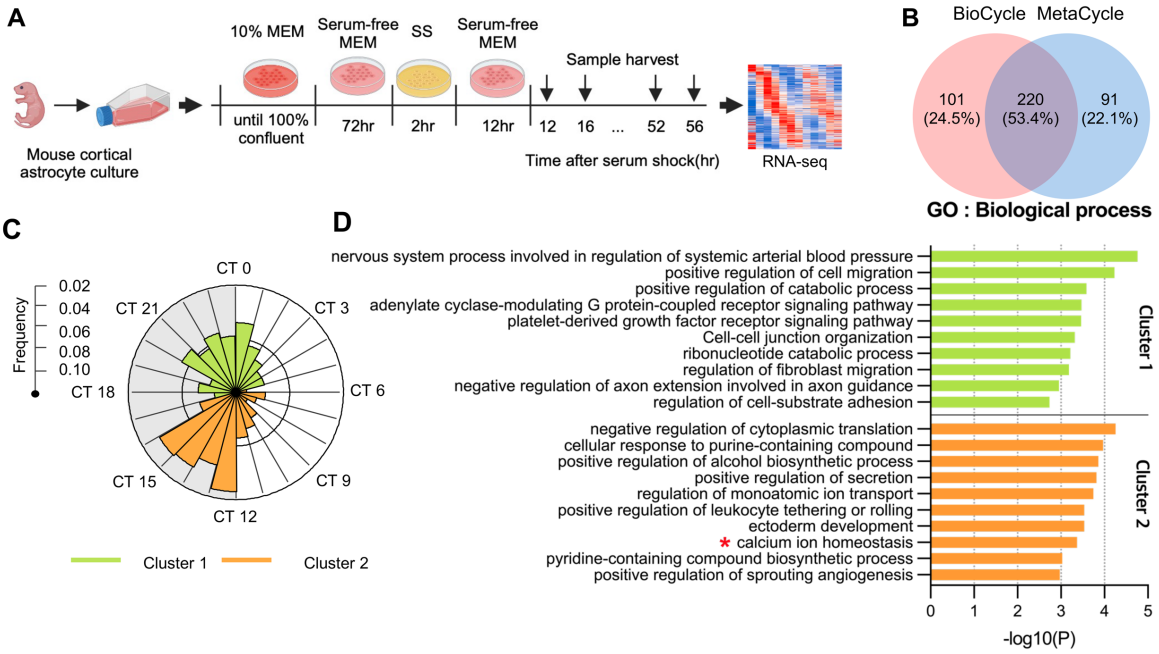

Figure 1. Circadian rhythmic transcripts in mouse cultured cortical astrocytes. (A) Experimental scheme for synchronizing circadian rhythms in mouse cultured cortical astrocytes culture with subsequent RNA-sequencing performed over 2 days. (B) Venn diagram displaying the number of circadian rhythmic transcripts identified by two algorithms ($q < 0.05$ in MetaCycle or BioCycle). (E) Expression profiles of *Plat*, *Il34*, *Adora1*, and *Mybph* in SS-synchronized cultured astrocytes obtained from RNA-seq data. The q-values for BioCycle (red) and MetaCycle (blue) are displayed in the bottom right corner. (C) Radial histogram of the distribution of phases of rhythmic genes in the astrocyte transcriptome. TASS was transformed to CT for ease of interpretation (TASS 8 hour = CT0). (D) Top 10 enriched GO Biological Process (BP) terms for significant astrocyte circadian rhythmic genes ($p < 0.01$) identified by Metascape (https://metascape.org). See also S1-S3 and Table S1.

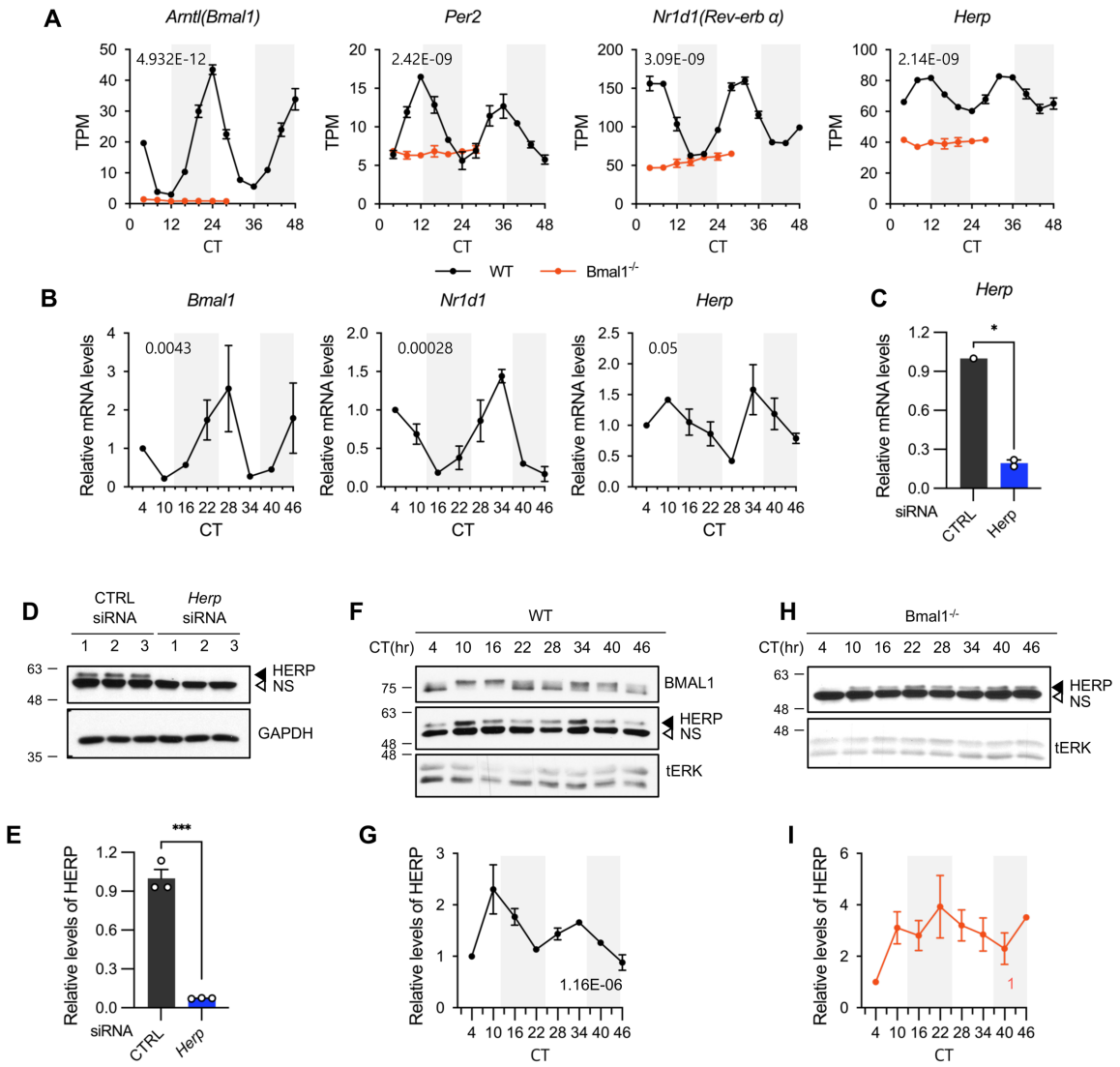

Figure 2. *Herp* is rhythmically expressed in mouse cultured astrocytes and its expression is controlled by BMAL1. (A, B) Select core clock genes exhibiting rhythmic expression in cultured astrocytes. Circadian clock-synchronized cultured astrocytes from WT (black) and *Bmal1*$^{-/-}$ (orange) mice were harvested at the indicated time (CT0 = TASS 8 hour). Expression was analyzed for rhythmicity using MetaCycle, and expression levels of given genes were quantified using RNA-seq (A) and real-time qRT-PCR (B) data. Values are means ± SEM (n = 2; p-values are indicated by insets in graphs). White and gray backgrounds represent subjective day and subjective night, respectively. (C - E) Assessment of *Herp* siRNA for use in characterizing anti-HERP antisera. Cultured astrocytes were transfected with the indicated siRNA (20nM) and processed for real-time qRT-PCR (C) and Western blot (D, E) analyses at 48 hours post transfection. (C) siRNA-mediated knockdown of *Herp* mRNA. Values are means ± SEM (n = 2; *p < 0.05, **p < 0.005, ***p < 0.0005, and ****p < 0.00005; independent *t*-test). (D) Representative Western blot image of HERP knockdown (from three independent experiments). GAPDH served as loading control. (E) Densitometric quantification of HERP levels, normalized to GAPDH levels. Values are means ± SEM (n = 3; ***p < 0.0005; Student's *t*-test). (F–I) BMAL1-dependence of HERP expression. Circadian clock-synchronized cultured astrocytes from WT (F, G) and *Bmal1*$^{-/-}$ (H, I) mice were harvested at the indicated times (CT0 = TASS 8 hours) and processed for Western blot analysis. HERP levels were normalized to total ERK (tERK), which served as a loading control. tERK values at different times were normalized to those at CT4 (defined as 1). P-values are indicated by insets in graphs. White and gray backgrounds represent subjective day and subjective night, respectively. (F, G) BMAL1 and HERP expression over time

in astrocytes from WT mice. (F) Representative Western blot image (from five independent experiments). (G) Densitometric quantification of Western blot data from WT mice. (H, I) BMAL1 and HERP expression over time in astrocytes from *Bmal1*$^{-/-}$ mice. (H) Representative Western blot image (from two independent experiments). (I) Densitometric quantification of Western blot data from *Bmal1*$^{-/-}$ mice.

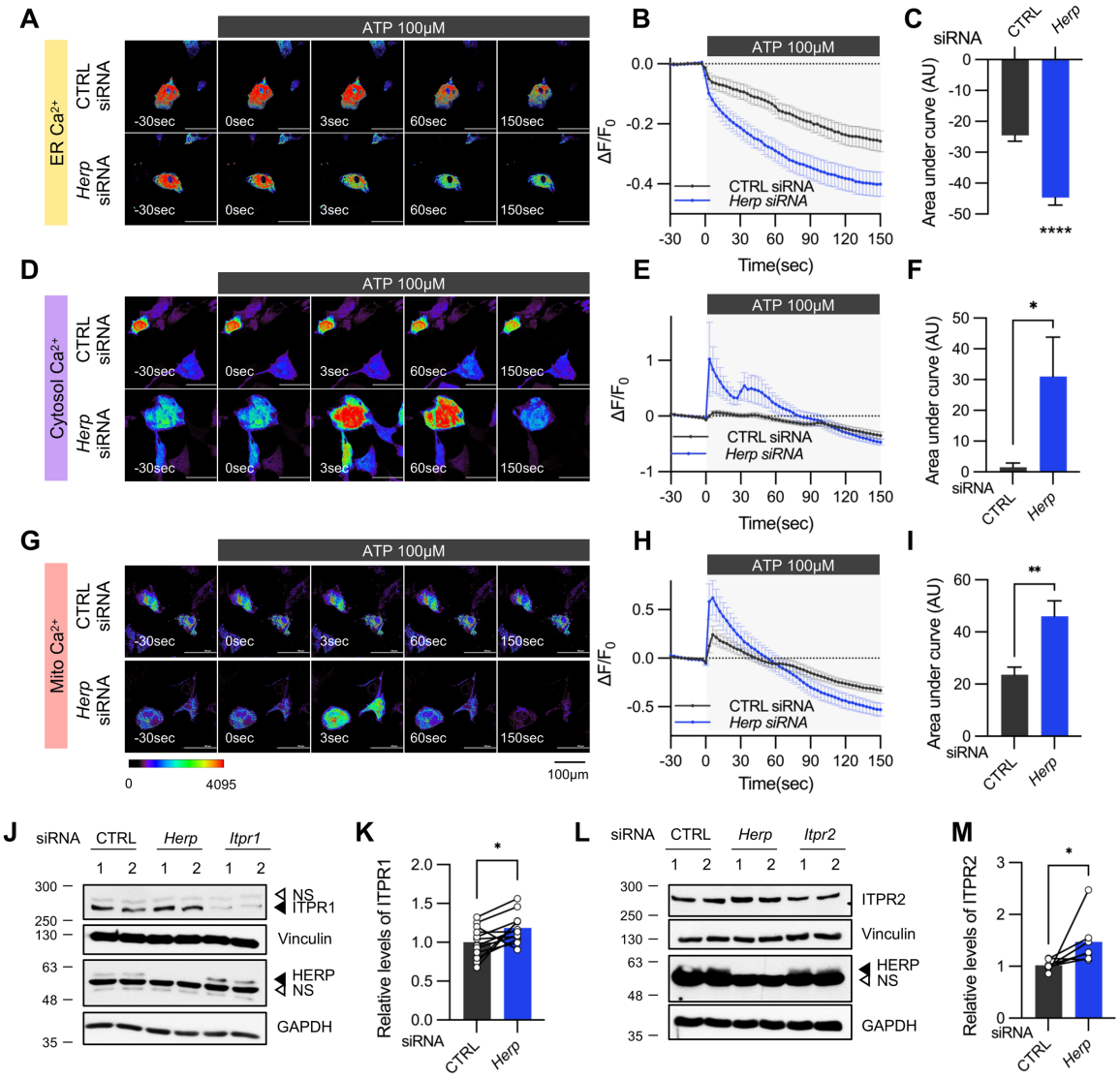

Figure 3. *Herp* knockdown altered ATP-induced ER Ca^{2+} response. (A-I) Imaging of subcellular ATP-induced Ca^{2+} signals in *Herp*-knockdown and control cultured astrocytes. Cultured astrocytes were co-transfected with 20 μM non-targeting (CTRL) siRNA or *Herp* siRNA together with ER (A–C), cytosol (D–F) or mitochondrial (Mito; G–I) compartment-specific Ca^{2+} indicator (denoted at left). At 48 hours post transfection, cultured astrocytes were stimulated with 100 μM ATP and Ca^{2+} imaging analysis was performed. Images were acquired every 3 seconds. (A, D, G) Representative time-lapse images of each Ca^{2+} indicator. (B, E, H) ΔF/F0 values over time following ATP application. (C, F, I) Area under the curve values, calculated from panels B, E, and H. (A–C) CTRL siRNA, n = 19; *Herp* siRNA, n = 22. (D–F) CTRL siRNA, n = 20; *Herp* siRNA, n = 25. (G–I) CTRL siRNA, n = 16; *Herp* siRNA, n = 16. (J–M) ITPR1 and ITPR2 protein levels in control and *Herp*-knockdown astrocytes. Cultured astrocytes were transfected with the indicated siRNA (20nM) and processed for Western blot analysis 48 hours after transfection. Vinculin and GAPDH served as loading control for ITPRs and HERP, respectively. (J and K) ITPR1 protein levels. *Itpr1* siRNA-transfected astrocytes were included as controls. (J) Representative Western blot image (from twelve independent experiments). (K) Densitometric quantification of Western blot data showing relative levels of ITPR1 in *Herp* siRNA-transfected astrocytes compared with CTRL siRNA transfected astrocytes. (L, M) ITPR2 protein levels. *Itpr2* siRNA-transfected astrocytes were included as controls. (L) Representative Western blot image (from five independent experiments). (M) Densitometric quantification

of Western blot data showing relative levels of ITPR2 in *Herp* siRNA-transfected astrocytes compared with CNTL astrocytes. Values in graphs are means ± SEM (*$p < 0.05$, **$p < 0.005$, ***$p < 0.0005$, ****$p < 0.00005$; independent *t*-test). See also S4.

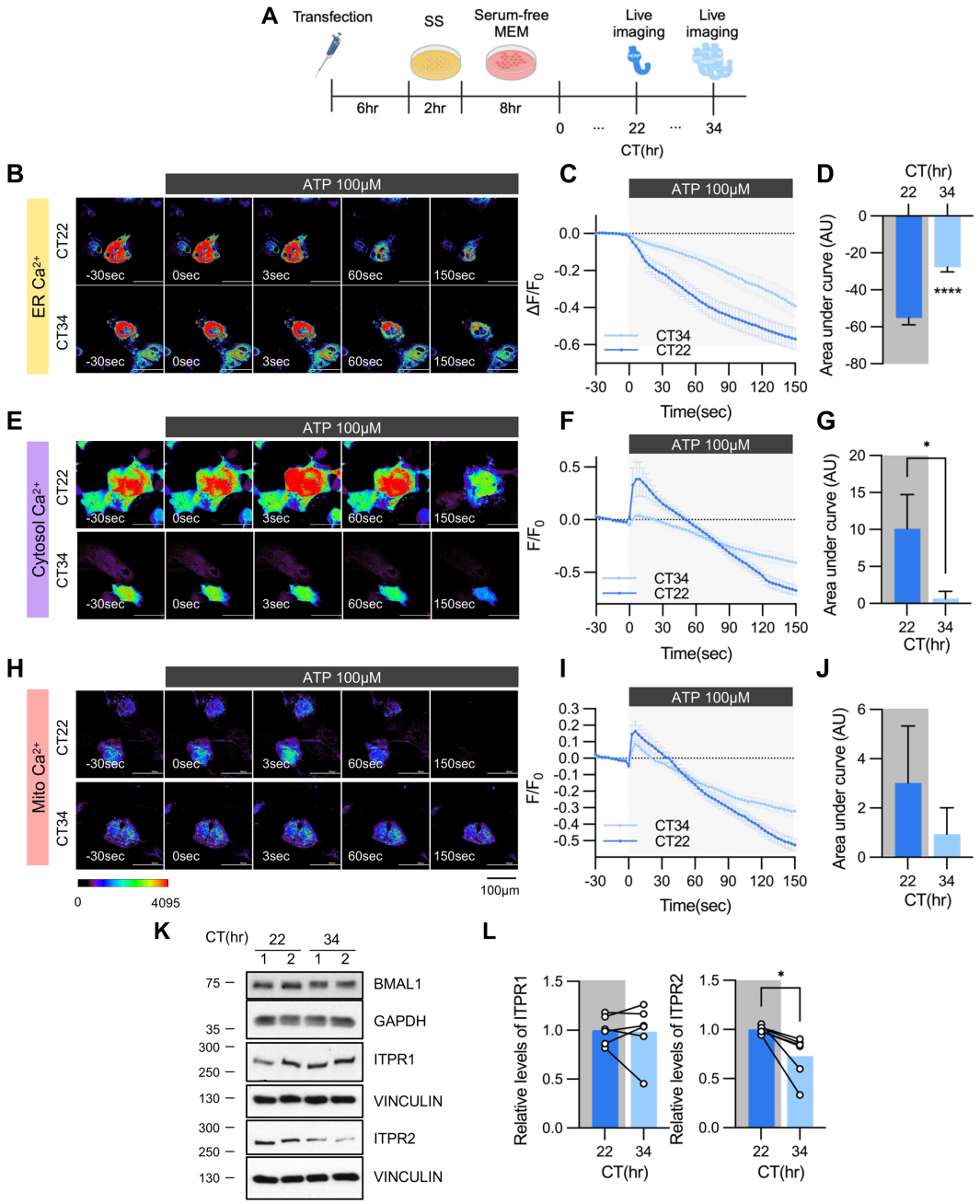

Figure 4. ATP-induced ER Ca^{2+} release varies according to CT. (A) Schematic depiction of experimental scheme from transfection to live-cell Ca^{2+} imaging at different CTs. (B–J) Imaging of subcellular ATP-induced Ca^{2+} signals in cultured astrocytes as a function of CT. Cultured astrocytes were transfected with ER (B–D), cytosolic (E–G) or mitochondrial (Mito; H–J) compartment-specific Ca^{2+} indicator (denoted at left) and then their circadian rhythm was synchronized by SS. At the indicated CT, astrocytes were stimulated with 100 μM ATP and Ca^{2+} imaging was performed. (B, E, H) Representative time-lapse images of each Ca^{2+} indicator. (C, F, I) $\Delta F/F_0$ values over time following ATP application. (D, G, J) Area under the curve values, calculated from panels C, F, and I. (B–D) CT22, n = 24; CT34 n = 19. (E–G) CT22, n = 33; CT34, n = 38. (H–J) CT22, n = 50; CT34, n = 54. (K, L) CT-dependent changes in ITPR1 and ITPR2. Cells were harvested at the indicated CTs and processed for Western blot analysis. Vinculin and GAPDH served as loading control for ITPR and BMAL1, respectively. (K) Representative Western blot image (from six

independent experiments). (L) Densitometric quantification of Western blot data showing relative levels of ITPR1 and ITPR2 at different CTs. Values in graphs are means ± SEMs (*$p < 0.05$, ****$p < 0.00005$; independent *t* test). See also S4.

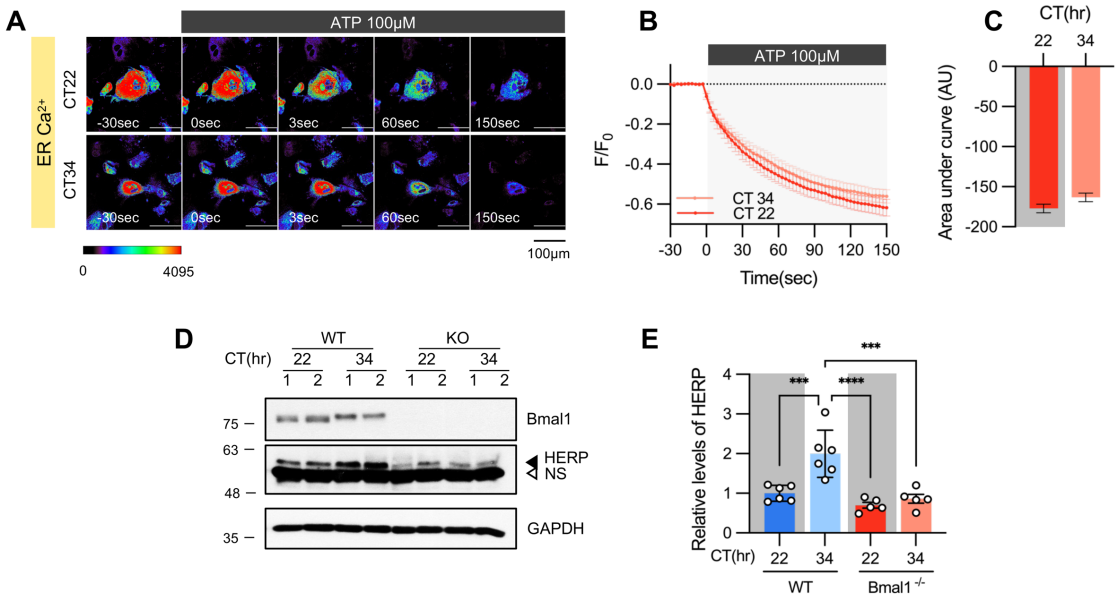

Figure 5. CT-dependent ER Ca^{2+} release is abolished in cultured astrocytes from *Bmal1*$^{-/-}$ mice. Cultured astrocytes from *Bmal1*$^{-/-}$ mice were transfected with ER Ca^{2+} indicator and then their circadian rhythm was synchronized by SS. At the indicated CTs, astrocytes were stimulated with 100 μM ATP and Ca^{2+} imaging was performed. (A) Representative time-lapse images of ER Ca^{2+} indicator. (B) $\Delta F/F_0$ values over time following ATP application. (C) Area under the curve values, calculated from panel B. (A–C) CT22, n = 34; CT34, n = 43. (D, E) Cultured astrocytes from *Bmal1*$^{-/-}$ mice and WT littermates were synchronized by SS. Cells were harvested at the indicated CTs and processed for Western blot analysis. (D) Representative Western blot image (from six independent experiments). GAPDH served as a loading control. (E) Relative levels of HERP in cultured astrocytes from *Bmal1*$^{-/-}$ mice and WT littermates at different CTs. Values are means ± SEM (*p < 0.05, **p < 0.005, ***p < 0.0005, ****p < 0.00005; repeated measures two-way ANOVA).

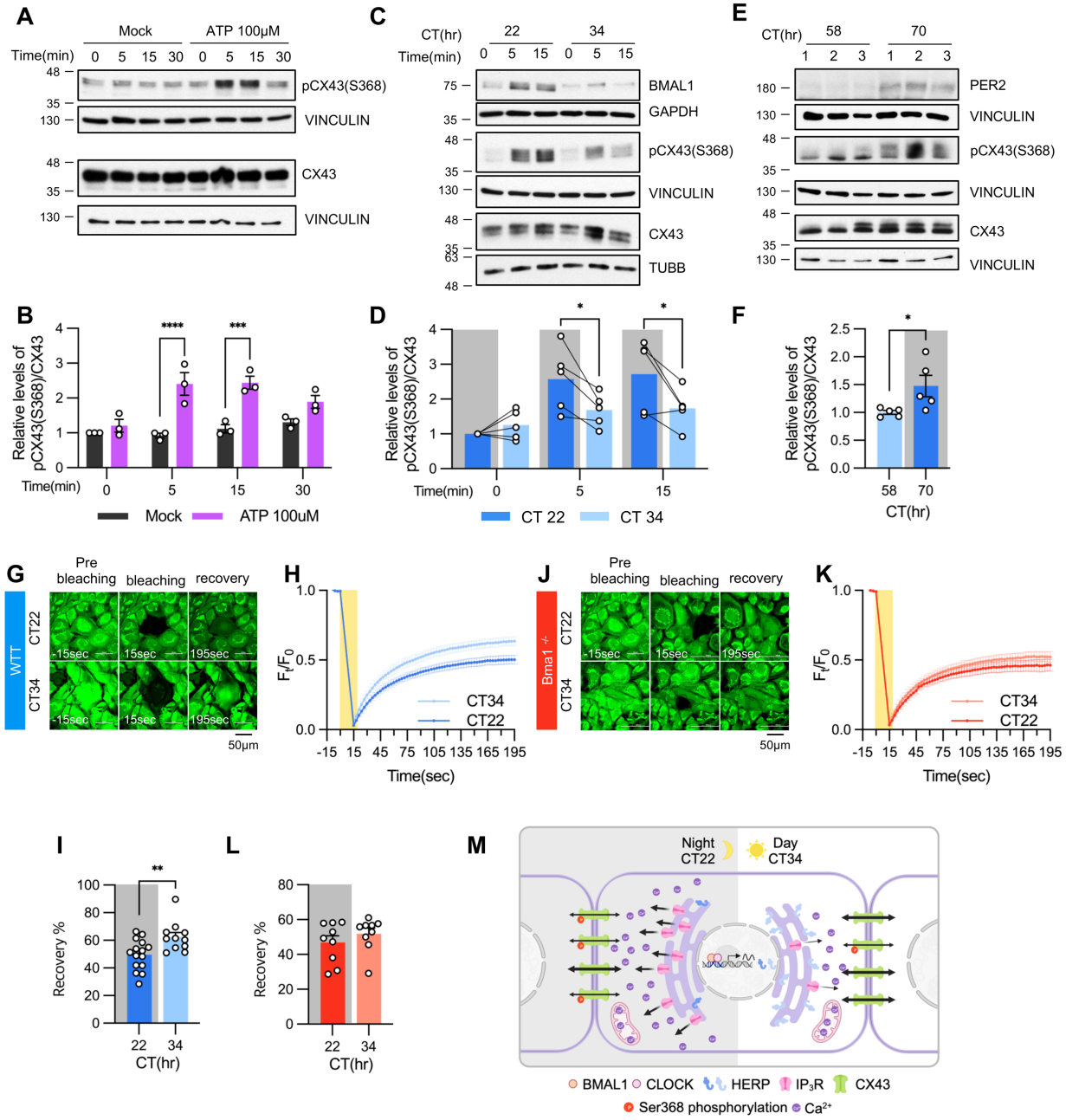

Figure 6. ATP-induced pCx43(S368) levels and the conductance of gap junctions varies according to CT. CT-dependent changes in phosphorylated Cx43 (pCx43). (A–D) Cultured astrocytes, with (C, D) or without (A, B), circadian clock synchronization were treated with 100 μM ATP and processed for Western blot analysis at the indicated times. Vinculin, GAPDH, and/or β-tubulin (TUBB) served as loading controls. The intensity of pCx43(S368) and Cx43 for each sample was normalized to that of Vinculin. (A, B) Cx43 phosphorylation in unsynchronized cultured astrocytes at different times (0, 5, 15, 30 minutes) after stimulation with ATP. (A) Representative Western blot image (from more than three independent experiments). Vinculin served as a loading control. (B) Densitometric quantification of Western blot data, showing relative pCx43(S368)/Cx43 levels. Values are normalized to those for mock-treated samples at time zero (defined as 1). (C, D) Cx43 phosphorylation in SS-synchronized cultured astrocytes at CT22 and CT34 at different times (0, 5, and 15 minutes) after stimulation with ATP. (C) Representative Western blot image (from more than three independent experiments). Vinculin, GAPDH, and β-tubulin (TUBB) served as

loading controls. (D) Densitometric quantification of Western blot data, showing relative pCx43(S368)/Cx43 levels. Values are normalized to those for mock-treated samples at time zero for CT22 (defined as 1). (E, F) Changes in Cx43 phosphorylation *in vivo*. Mice were entrained to a 12-hour light/dark cycle followed by constant dark conditions. At the indicated CTs, the prefrontal cortex area was dissected and processed for Western blot analysis. (E) Representative Western blot image (from three independent experiments). (E) Densitometric quantification of Western blot data showing relative levels of pCx43(S368). (G-L) Circadian rhythm of cultured astrocytes from (G-I) WT and (J-L) Bmal1$^{-/-}$ mice were synchronized by SS. At the indicated CT, gap-FRAP was performed. (G and J) Representative time-lapse images of prebleaching, bleaching and recovery condition during gap-FRAP analysis at CT22 and CT34. (H and K) F_t/F_0 values over time following photobleaching (yellow rectangle). (I and L) Recovery % values, calculated from panel H and L, respectively. (G-L) CT22, n = 15; CT34, n = 11. (J-L) CT22, n = 9; CT34, n = 9. Values in graphs are means ± SEMs (*p < 0.05, **p < 0.005, ***p < 0.0005, and ****p < 0.00005; independent *t*-test). See also S5-S6.

References

Agostinelli, F., Ceglia, N., Shahbaba, B., Sassone-Corsi, P., & Baldi, P. (2016). What time is it? Deep learning approaches for circadian rhythms. *Bioinformatics*, *32*(12), i8-i17. https://doi.org/10.1093/bioinformatics/btw243

Agulhon, C., Petravicz, J., McMullen, A. B., Sweger, E. J., Minton, S. K., Taves, S. R., Casper, K. B., Fiacco, T. A., & McCarthy, K. D. (2008). What Is the Role of Astrocyte Calcium in Neurophysiology? *Neuron*, *59*(6), 932-946. https://doi.org/https://doi.org/10.1016/j.neuron.2008.09.004

Annayev, Y., Adar, S., Chiou, Y. Y., Lieb, J. D., Sancar, A., & Ye, R. (2014). Gene model 129 (Gm129) encodes a novel transcriptional repressor that modulates circadian gene expression. *J Biol Chem*, *289*(8), 5013-5024. https://doi.org/10.1074/jbc.M113.534651

Balsalobre, A., Damiola, F., & Schibler, U. (1998). A serum shock induces circadian gene expression in mammalian tissue culture cells. *Cell*, *93*(6), 929-937. https://doi.org/10.1016/s0092-8674(00)81199-x

Barca-Mayo, O., Boender, A. J., Armirotti, A., & De Pietri Tonelli, D. (2020). Deletion of astrocytic BMAL1 results in metabolic imbalance and shorter lifespan in mice. *Glia*, *68*(6), 1131-1147. https://doi.org/10.1002/glia.23764

Barca-Mayo, O., Pons-Espinal, M., Follert, P., Armirotti, A., Berdondini, L., & De Pietri Tonelli, D. (2017). Astrocyte deletion of Bmal1 alters daily locomotor activity and cognitive functions via GABA signalling. *Nat Commun*, *8*, 14336. https://doi.org/10.1038/ncomms14336

Baryshnikov, S. G., Rogachevskaja, O. A., & Kolesnikov, S. S. (2003). Calcium signaling mediated by P2Y receptors in mouse taste cells. *J Neurophysiol*, *90*(5), 3283-3294. https://doi.org/10.1152/jn.00312.2003

Bell-Pedersen, D., Cassone, V. M., Earnest, D. J., Golden, S. S., Hardin, P. E., Thomas, T. L., & Zoran, M. J. (2005). Circadian rhythms from multiple oscillators: lessons from diverse organisms. *Nat Rev Genet*, *6*(7), 544-556. https://doi.org/10.1038/nrg1633

Blum, I. D., Keleş, M. F., Baz, E. S., Han, E., Park, K., Luu, S., Issa, H., Brown, M., Ho, M. C. W., Tabuchi, M., Liu, S., & Wu, M. N. (2021). Astroglial Calcium Signaling Encodes Sleep Need in Drosophila. *Curr Biol*, *31*(1), 150-162.e157. https://doi.org/10.1016/j.cub.2020.10.012

Bojarskaite, L., Bjornstad, D. M., Pettersen, K. H., Cunen, C., Hermansen, G. H., Abjorsbraten, K. S., Chambers, A. R., Sprengel, R., Vervaeke, K., Tang, W., Enger, R., & Nagelhus, E. A. (2020). Astrocytic Ca(2+) signaling is reduced during sleep and is involved in the regulation of slow wave sleep. *Nat Commun*, *11*(1), 3240. https://doi.org/10.1038/s41467-020-17062-2

Brancaccio, M., Edwards, M. D., Patton, A. P., Smyllie, N. J., Chesham, J. E., Maywood, E. S., & Hastings, M. H. (2019). Cell-autonomous clock of astrocytes drives circadian behavior in mammals. *Science*, *363*(6423), 187-192. https://doi.org/10.1126/science.aat4104

Brancaccio, M., Patton, A. P., Chesham, J. E., Maywood, E. S., & Hastings, M. H. (2017). Astrocytes Control Circadian Timekeeping in the Suprachiasmatic Nucleus via Glutamatergic Signaling. *Neuron*, *93*(6), 1420-1435 e1425. https://doi.org/10.1016/j.neuron.2017.02.030

Brandebura, A. N., Paumier, A., Onur, T. S., & Allen, N. J. (2023). Astrocyte contribution to dysfunction, risk and progression in neurodegenerative disorders. *Nature Reviews Neuroscience*, *24*(1), 23-39. https://doi.org/10.1038/s41583-022-00641-1

Bunger, M. K., Wilsbacher, L. D., Moran, S. M., Clendenin, C., Radcliffe, L. A., Hogenesch, J. B., Simon, M. C., Takahashi, J. S., & Bradfield, C. A. (2000). Mop3 is an essential component of the master circadian pacemaker in mammals. *Cell*, *103*(7), 1009-1017. https://doi.org/10.1016/s0092-8674(00)00205-1

Choi, D. J., Eun, J. H., Kim, B. G., Jou, I., Park, S. M., & Joe, E. H. (2018). A Parkinson's disease gene, DJ-1, repairs brain injury through Sox9 stabilization and astrogliosis. *Glia*, *66*(2), 445-458. https://doi.org/10.1002/glia.23258

Dobin, A., Davis, C. A., Schlesinger, F., Drenkow, J., Zaleski, C., Jha, S., Batut, P., Chaisson, M., & Gingeras, T. R. (2013). STAR: ultrafast universal RNA-seq aligner. *Bioinformatics*, *29*(1), 15-21. https://doi.org/10.1093/bioinformatics/bts635

Dunham, I., Kundaje, A., Aldred, S. F., Collins, P. J., Davis, C. A., Doyle, F., Epstein, C. B., Frietze, S., Harrow, J., Kaul, R., Khatun, J., Lajoie, B. R., Landt, S. G., Lee, B.-K., Pauli, F., Rosenbloom, K. R., Sabo, P., Safi, A., Sanyal, A., . . . HudsonAlpha Institute, C. U. C. I. S. g. (2012). An integrated encyclopedia of DNA elements in the human genome. *Nature*, *489*(7414), 57-74. https://doi.org/10.1038/nature11247

Enkvist, M. O., & McCarthy, K. D. (1992). Activation of protein kinase C blocks astroglial gap junction communication and inhibits the spread of calcium waves. *J Neurochem*, *59*(2), 519-526. https://doi.org/10.1111/j.1471-4159.1992.tb09401.x

Fróes, M. M., Correia, A. H., Garcia-Abreu, J., Spray, D. C., Campos de Carvalho, A. C., & Neto, M. V. (1999). Gap-junctional coupling between neurons and astrocytes in primary central nervous system cultures. *Proc Natl Acad Sci U S A*, *96*(13), 7541-7546. https://doi.org/10.1073/pnas.96.13.7541

Fujii, Y., Maekawa, S., & Morita, M. (2017). Astrocyte calcium waves propagate proximally by gap junction and distally by extracellular diffusion of ATP released from volume-regulated anion channels. *Scientific Reports*, *7*(1), 13115. https://doi.org/10.1038/s41598-017-13243-0

Giaume, C., Koulakoff, A., Roux, L., Holcman, D., & Rouach, N. (2010). Astroglial networks: a step further in neuroglial and gliovascular interactions. *Nat Rev Neurosci*, *11*(2), 87-99. https://doi.org/10.1038/nrn2757

Giaume, C., Naus, C. C., Sáez, J. C., & Leybaert, L. (2021). Glial Connexins and Pannexins in the Healthy and Diseased Brain. *Physiol Rev*, *101*(1), 93-145. https://doi.org/10.1152/physrev.00043.2018

Giorgi, C., Marchi, S., & Pinton, P. (2018). The machineries, regulation and cellular functions of mitochondrial calcium. *Nature Reviews Molecular Cell Biology*, *19*(11), 713-730. https://doi.org/10.1038/s41580-018-0052-8

Griemsmann, S., Höft, S. P., Bedner, P., Zhang, J., von Staden, E., Beinhauer, A., Degen, J., Dublin, P., Cope, D. W., Richter, N., Crunelli, V., Jabs, R., Willecke, K., Theis, M., Seifert, G., Kettenmann, H., & Steinhäuser, C. (2015). Characterization of Panglial Gap Junction Networks in the Thalamus, Neocortex, and Hippocampus Reveals a Unique Population of Glial Cells. *Cereb Cortex*, *25*(10), 3420-3433. https://doi.org/10.1093/cercor/bhu157

Griffin, P., Dimitry, J. M., Sheehan, P. W., Lananna, B. V., Guo, C., Robinette, M. L., Hayes, M. E., Cedeno, M. R., Nadarajah, C. J., Ezerskiy, L. A., Colonna, M., Zhang, J., Bauer, A. Q., Burris, T. P., & Musiek, E. S. (2019). Circadian clock protein Rev-erbalpha regulates neuroinflammation. *Proc Natl Acad Sci U S A*, *116*(11), 5102-5107. https://doi.org/10.1073/pnas.1812405116

Guerra-Gomes, S., Sousa, N., Pinto, L., & Oliveira, J. F. (2017). Functional Roles of Astrocyte Calcium Elevations: From Synapses to Behavior. *Front Cell Neurosci*, *11*, 427. https://doi.org/10.3389/fncel.2017.00427

Holtzclaw, L. A., Pandhit, S., Bare, D. J., Mignery, G. A., & Russell, J. T. (2002). Astrocytes in adult rat brain express type 2 inositol 1,4,5-trisphosphate receptors. *Glia*, *39*(1), 69-84. https://doi.org/10.1002/glia.10085

Hong, H. K., Maury, E., Ramsey, K. M., Perelis, M., Marcheva, B., Omura, C., Kobayashi, Y., Guttridge, D. C., Barish, G. D., & Bass, J. (2018). Requirement for NF-κB in maintenance of molecular and behavioral circadian rhythms in mice. *Genes Dev*, *32*(21-22), 1367-1379. https://doi.org/10.1101/gad.319228.118

Hoyle, N. P., Seinkmane, E., Putker, M., Feeney, K. A., Krogager, T. P., Chesham, J. E., Bray, L. K., Thomas, J. M., Dunn, K., Blaikley, J., & O'Neill, J. S. (2017). Circadian actin dynamics drive

rhythmic fibroblast mobilization during wound healing. *Sci Transl Med*, *9*(415). https://doi.org/10.1126/scitranslmed.aal2774

Ingiosi, A. M., Hayworth, C. R., Harvey, D. O., Singletary, K. G., Rempe, M. J., Wisor, J. P., & Frank, M. G. (2020). A Role for Astroglial Calcium in Mammalian Sleep and Sleep Regulation. *Curr Biol*, *30*(22), 4373-4383.e4377. https://doi.org/10.1016/j.cub.2020.08.052

James, G., & Butt, A. M. (2001). P2X and P2Y purinoreceptors mediate ATP-evoked calcium signalling in optic nerve glia in situ. *Cell Calcium*, *30*(4), 251-259. https://doi.org/10.1054/ceca.2001.0232

Kiyoshi, C. M., & Zhou, M. (2019). Astrocyte syncytium: a functional reticular system in the brain. *Neural Regen Res*, *14*(4), 595-596. https://doi.org/10.4103/1673-5374.247462

Kokame, K., Agarwala, K. L., Kato, H., & Miyata, T. (2000). Herp, a new ubiquitin-like membrane protein induced by endoplasmic reticulum stress. *J Biol Chem*, *275*(42), 32846-32853. https://doi.org/10.1074/jbc.M002063200

Kokame, K., Kato, H., & Miyata, T. (1996). Homocysteine-respondent genes in vascular endothelial cells identified by differential display analysis. GRP78/BiP and novel genes. *J Biol Chem*, *271*(47), 29659-29665. https://doi.org/10.1074/jbc.271.47.29659

Kunzelmann, P., Schroder, W., Traub, O., Steinhauser, C., Dermietzel, R., & Willecke, K. (1999). Late onset and increasing expression of the gap junction protein connexin30 in adult murine brain and long-term cultured astrocytes. *Glia*, *25*(2), 111-119. https://doi.org/10.1002/(sici)1098-1136(19990115)25:2<111::aid-glia2>3.0.co;2-i

Lananna, B. V., & Musiek, E. S. (2020). The wrinkling of time: Aging, inflammation, oxidative stress, and the circadian clock in neurodegeneration. *Neurobiol Dis*, *139*, 104832. https://doi.org/10.1016/j.nbd.2020.104832

Lananna, B. V., Nadarajah, C. J., Izumo, M., Cedeno, M. R., Xiong, D. D., Dimitry, J., Tso, C. F., McKee, C. A., Griffin, P., Sheehan, P. W., Haspel, J. A., Barres, B. A., Liddelow, S. A., Takahashi, J. S., Karatsoreos, I. N., & Musiek, E. S. (2018). Cell-Autonomous Regulation of Astrocyte Activation by the Circadian Clock Protein BMAL1. *Cell Rep*, *25*(1), 1-9 e5. https://doi.org/10.1016/j.celrep.2018.09.015

Langer, J., Stephan, J., Theis, M., & Rose, C. R. (2012). Gap junctions mediate intercellular spread of sodium between hippocampal astrocytes in situ. *Glia*, *60*(2), 239-252. https://doi.org/10.1002/glia.21259

Leitman, J., Shenkman, M., Gofman, Y., Shtern, N. O., Ben-Tal, N., Hendershot, L. M., & Lederkremer, G. Z. (2014). Herp coordinates compartmentalization and recruitment of HRD1 and misfolded proteins for ERAD. *Mol Biol Cell*, *25*(7), 1050-1060. https://doi.org/10.1091/mbc.E13-06-0350

Liu, T.-T., Kim, S., Desai, P., Kim, D.-H., Huang, X., Ferris, S. T., Wu, R., Ou, F., Egawa, T., Van Dyken, S. J., Diamond, M. S., Johnson, P. F., Kubo, M., Murphy, T. L., & Murphy, K. M. (2022). Ablation of cDC2 development by triple mutations within the Zeb2 enhancer. *Nature*, *607*(7917), 142-148. https://doi.org/10.1038/s41586-022-04866-z

Marpegan, L., Krall, T. J., & Herzog, E. D. (2009). Vasoactive intestinal polypeptide entrains circadian rhythms in astrocytes. *J Biol Rhythms*, *24*(2), 135-143. https://doi.org/10.1177/0748730409332042

Mohawk, J. A., Green, C. B., & Takahashi, J. S. (2012). Central and peripheral circadian clocks in mammals. *Annu Rev Neurosci*, *35*, 445-462. https://doi.org/10.1146/annurev-neuro-060909-153128

Mure, L. S., Le, H. D., Benegiamo, G., Chang, M. W., Rios, L., Jillani, N., Ngotho, M., Kariuki, T., Dkhissi-Benyahya, O., Cooper, H. M., & Panda, S. (2018). Diurnal transcriptome atlas of a primate across major neural and peripheral tissues. *Science*, *359*(6381). https://doi.org/10.1126/science.aao0318

Nagy, J. I., Patel, D., Ochalski, P. A., & Stelmack, G. L. (1999). Connexin30 in rodent, cat and human brain: selective expression in gray matter astrocytes, co-localization with connexin43 at gap junctions and late developmental appearance. *Neuroscience*, *88*(2), 447-468. https://doi.org/10.1016/s0306-4522(98)00191-2

Neary, J. T., van Breemen, C., Forster, E., Norenberg, L. O., & Norenberg, M. D. (1988). ATP stimulates calcium influx in primary astrocyte cultures. *Biochem Biophys Res Commun*, *157*(3), 1410-1416. https://doi.org/10.1016/s0006-291x(88)81032-5

Nimlamool, W., Andrews, R. M., & Falk, M. M. (2015). Connexin43 phosphorylation by PKC and MAPK signals VEGF-mediated gap junction internalization. *Mol Biol Cell*, *26*(15), 2755-2768. https://doi.org/10.1091/mbc.E14-06-1105

Oki, S., Ohta, T., Shioi, G., Hatanaka, H., Ogasawara, O., Okuda, Y., Kawaji, H., Nakaki, R., Sese, J., & Meno, C. (2018). ChIP-Atlas: a data-mining suite powered by full integration of public ChIP-seq data. *EMBO reports*, *19*(12), e46255. https://doi.org/https://doi.org/10.15252/embr.201846255

Outinen, P. A., Sood, S. K., Pfeifer, S. I., Pamidi, S., Podor, T. J., Li, J., Weitz, J. I., & Austin, R. C. (1999). Homocysteine-Induced Endoplasmic Reticulum Stress and Growth Arrest Leads to Specific Changes in Gene Expression in Human Vascular Endothelial Cells. *Blood*, *94*(3), 959-967. https://doi.org/https://doi.org/10.1182/blood.V94.3.959.415k20_959_967

Pacholko, A. G., Wotton, C. A., & Bekar, L. K. (2020). Astrocytes—The Ultimate Effectors of Long-Range Neuromodulatory Networks? [Review]. *Frontiers in Cellular Neuroscience*, *14*. https://doi.org/10.3389/fncel.2020.581075

Panda, S., Antoch, M. P., Miller, B. H., Su, A. I., Schook, A. B., Straume, M., Schultz, P. G., Kay, S. A., Takahashi, J. S., & Hogenesch, J. B. (2002). Coordinated transcription of key pathways in the mouse by the circadian clock. *Cell*, *109*(3), 307-320. https://doi.org/10.1016/s0092-8674(02)00722-5

Paredes, F., Parra, V., Torrealba, N., Navarro-Marquez, M., Gatica, D., Bravo-Sagua, R., Troncoso, R., Pennanen, C., Quiroga, C., Chiong, M., Caesar, C., Taylor, W. R., Molgó, J., San Martin, A., Jaimovich, E., & Lavandero, S. (2016). HERPUD1 protects against oxidative stress-induced apoptosis through downregulation of the inositol 1,4,5-trisphosphate receptor. *Free Radic Biol Med*, *90*, 206-218. https://doi.org/10.1016/j.freeradbiomed.2015.11.024

Patton, A. P., Smyllie, N. J., Chesham, J. E., & Hastings, M. H. (2022). Astrocytes sustain circadian oscillation and bidirectionally determine circadian period, but do not regulate circadian phase in the suprachiasmatic nucleus. *J Neurosci*, *42*(28), 5522-5537. https://doi.org/10.1523/jneurosci.2337-21.2022

Pekny, M., & Pekna, M. (2016). Reactive gliosis in the pathogenesis of CNS diseases. *Biochimica et Biophysica Acta (BBA) - Molecular Basis of Disease*, *1862*(3), 483-491. https://doi.org/https://doi.org/10.1016/j.bbadis.2015.11.014

Phatnani, H., & Maniatis, T. (2015). Astrocytes in neurodegenerative disease. *Cold Spring Harb Perspect Biol*, *7*(6). https://doi.org/10.1101/cshperspect.a020628

Pogoda, K., Kameritsch, P., Retamal, M. A., & Vega, J. L. (2016). Regulation of gap junction channels and hemichannels by phosphorylation and redox changes: a revision. *BMC Cell Biol*, *17 Suppl 1*(Suppl 1), 11. https://doi.org/10.1186/s12860-016-0099-3

Prolo, L. M., Takahashi, J. S., & Herzog, E. D. (2005). Circadian Rhythm Generation and Entrainment in Astrocytes. *The Journal of Neuroscience*, *25*(2), 404-408. https://doi.org/10.1523/jneurosci.4133-04.2005

Pun, R., Kim, M. H., & North, B. J. (2022). Role of Connexin 43 phosphorylation on Serine-368 by PKC in cardiac function and disease. *Front Cardiovasc Med*, *9*, 1080131. https://doi.org/10.3389/fcvm.2022.1080131

Rakshit, K., Qian, J., Ernst, J., & Matveyenko, A. V. (2016). Circadian variation of the pancreatic islet transcriptome. *Physiological Genomics*, *48*(9), 677-687. https://doi.org/10.1152/physiolgenomics.00019.2016

Rash, J. E., Duffy, H. S., Dudek, F. E., Bilhartz, B. L., Whalen, L. R., & Yasumura, T. (1997). Grid-mapped freeze-fracture analysis of gap junctions in gray and white matter of adult rat central nervous system, with evidence for a "panglial syncytium" that is not coupled to neurons. *J Comp Neurol*, *388*(2), 265-292. https://doi.org/10.1002/(sici)1096-9861(19971117)388:2<265::aid-cne6>3.0.co;2-#

Reddy, A. B., Karp, N. A., Maywood, E. S., Sage, E. A., Deery, M., O'Neill, J. S., Wong, G. K., Chesham, J., Odell, M., Lilley, K. S., Kyriacou, C. P., & Hastings, M. H. (2006). Circadian orchestration of the hepatic proteome. *Curr Biol*, *16*(11), 1107-1115. https://doi.org/10.1016/j.cub.2006.04.026

Reinke, H., & Asher, G. (2019). Crosstalk between metabolism and circadian clocks. *Nat Rev Mol Cell Biol*, *20*(4), 227-241. https://doi.org/10.1038/s41580-018-0096-9

Santiquet, N. W., Develle, Y., Laroche, A., Robert, C., & Richard, F. J. (2012). Regulation of gap-junctional communication between cumulus cells during in vitro maturation in swine, a gap-FRAP study. *Biol Reprod*, *87*(2), 46. https://doi.org/10.1095/biolreprod.112.099754

Schultz, T. F., & Kay, S. A. (2003). Circadian clocks in daily and seasonal control of development. *Science*, *301*(5631), 326-328. https://doi.org/10.1126/science.1085935

Semyanov, A., Henneberger, C., & Agarwal, A. (2020). Making sense of astrocytic calcium signals — from acquisition to interpretation. *Nature Reviews Neuroscience*, *21*(10), 551-564. https://doi.org/10.1038/s41583-020-0361-8

Sharp, A. H., Nucifora, F. C., Jr., Blondel, O., Sheppard, C. A., Zhang, C., Snyder, S. H., Russell, J. T., Ryugo, D. K., & Ross, C. A. (1999). Differential cellular expression of isoforms of inositol 1,4,5-triphosphate receptors in neurons and glia in brain. *J Comp Neurol*, *406*(2), 207-220.

Sherwood, M. W., Arizono, M., Panatier, A., Mikoshiba, K., & Oliet, S. H. R. (2021). Astrocytic IP(3)Rs: Beyond IP(3)R2. *Front Cell Neurosci*, *15*, 695817. https://doi.org/10.3389/fncel.2021.695817

Sofroniew, M. V., & Vinters, H. V. (2010). Astrocytes: biology and pathology. *Acta Neuropathol*, *119*(1), 7-35. https://doi.org/10.1007/s00401-009-0619-8

Solan, J. L., & Lampe, P. D. (2014). Specific Cx43 phosphorylation events regulate gap junction turnover in vivo. *FEBS Lett*, *588*(8), 1423-1429. https://doi.org/10.1016/j.febslet.2014.01.049

Solan, J. L., & Lampe, P. D. (2016). Kinase programs spatiotemporally regulate gap junction assembly and disassembly: Effects on wound repair. *Semin Cell Dev Biol*, *50*, 40-48. https://doi.org/10.1016/j.semcdb.2015.12.010

Suzuki, J., Kanemaru, K., Ishii, K., Ohkura, M., Okubo, Y., & Iino, M. (2014). Imaging intraorganellar Ca2+ at subcellular resolution using CEPIA. *Nat Commun*, *5*, 4153. https://doi.org/10.1038/ncomms5153

Szabó, Z., Héja, L., Szalay, G., Kékesi, O., Füredi, A., Szebényi, K., Dobolyi, Á., Orbán, T. I., Kolacsek, O., Tompa, T., Miskolczy, Z., Biczók, L., Rózsa, B., Sarkadi, B., & Kardos, J. (2017). Extensive astrocyte synchronization advances neuronal coupling in slow wave activity in vivo. *Scientific Reports*, *7*(1), 6018. https://doi.org/10.1038/s41598-017-06073-7

Takahashi, J. S. (2017). Transcriptional architecture of the mammalian circadian clock. *Nat Rev Genet*, *18*(3), 164-179. https://doi.org/10.1038/nrg.2016.150

Torrealba, N., Navarro-Marquez, M., Garrido, V., Pedrozo, Z., Romero, D., Eura, Y., Villalobos, E., Roa, J. C., Chiong, M., Kokame, K., & Lavandero, S. (2017). Herpud1 negatively regulates pathological cardiac hypertrophy by inducing IP3 receptor degradation. *Sci Rep*, *7*(1), 13402. https://doi.org/10.1038/s41598-017-13797-z

Tso, C. F., Simon, T., Greenlaw, A. C., Puri, T., Mieda, M., & Herzog, E. D. (2017). Astrocytes Regulate Daily Rhythms in the Suprachiasmatic Nucleus and Behavior. *Current Biology*, *27*(7), 1055-1061. https://doi.org/https://doi.org/10.1016/j.cub.2017.02.037

Tsunematsu, T., Sakata, S., Sanagi, T., Tanaka, K. F., & Matsui, K. (2021). Region-specific and state-dependent astrocyte Ca²⁺ dynamics during the sleep-wake cycle in mice. *The Journal of Neuroscience*, JN-RM-2912-2920. https://doi.org/10.1523/jneurosci.2912-20.2021

Verkhratsky, A., & Nedergaard, M. (2018). Physiology of Astroglia. *Physiol Rev*, *98*(1), 239-389. https://doi.org/10.1152/physrev.00042.2016

Vyazovskiy, V. V., Olcese, U., Lazimy, Y. M., Faraguna, U., Esser, S. K., Williams, J. C., Cirelli, C., & Tononi, G. (2009). Cortical firing and sleep homeostasis. *Neuron*, *63*(6), 865-878. https://doi.org/10.1016/j.neuron.2009.08.024

Wen, S., Ma, D., Zhao, M., Xie, L., Wu, Q., Gou, L., Zhu, C., Fan, Y., Wang, H., & Yan, J. (2020). Spatiotemporal single-cell analysis of gene expression in the mouse suprachiasmatic nucleus. *Nat Neurosci*, *23*(3), 456-467. https://doi.org/10.1038/s41593-020-0586-x

Wu, G., Anafi, R. C., Hughes, M. E., Kornacker, K., & Hogenesch, J. B. (2016). MetaCycle: an integrated R package to evaluate periodicity in large scale data. *Bioinformatics*, *32*(21), 3351-3353. https://doi.org/10.1093/bioinformatics/btw405

Wu, J., Liu, L., Matsuda, T., Zhao, Y., Rebane, A., Drobizhev, M., Chang, Y. F., Araki, S., Arai, Y., March, K., Hughes, T. E., Sagou, K., Miyata, T., Nagai, T., Li, W. H., & Campbell, R. E. (2013). Improved orange and red Ca^{2}± indicators and photophysical considerations for optogenetic applications. *ACS Chem Neurosci*, *4*(6), 963-972. https://doi.org/10.1021/cn400012b

Yoshitane, H., Asano, Y., Sagami, A., Sakai, S., Suzuki, Y., Okamura, H., Iwasaki, W., Ozaki, H., & Fukada, Y. (2019). Functional D-box sequences reset the circadian clock and drive mRNA rhythms. *Commun Biol*, *2*, 300. https://doi.org/10.1038/s42003-019-0522-3

Yoshitane, H., Takao, T., Satomi, Y., Du, N. H., Okano, T., & Fukada, Y. (2009). Roles of CLOCK phosphorylation in suppression of E-box-dependent transcription. *Mol Cell Biol*, *29*(13), 3675-3686. https://doi.org/10.1128/mcb.01864-08

Zhang, R., Lahens, N. F., Ballance, H. I., Hughes, M. E., & Hogenesch, J. B. (2014). A circadian gene expression atlas in mammals: implications for biology and medicine. *Proc Natl Acad Sci U S A*, *111*(45), 16219-16224. https://doi.org/10.1073/pnas.1408886111

Zhao, Y., Araki, S., Wu, J., Teramoto, T., Chang, Y. F., Nakano, M., Abdelfattah, A. S., Fujiwara, M., Ishihara, T., Nagai, T., & Campbell, R. E. (2011). An expanded palette of genetically encoded Ca^{2+} indicators. *Science*, *333*(6051), 1888-1891. https://doi.org/10.1126/science.1208592

Zhou, Y., Zhou, B., Pache, L., Chang, M., Khodabakhshi, A. H., Tanaseichuk, O., Benner, C., & Chanda, S. K. (2019). Metascape provides a biologist-oriented resource for the analysis of systems-level datasets. *Nat Commun*, *10*(1), 1523. https://doi.org/10.1038/s41467-019-09234-6

Zou, Z., Ohta, T., Miura, F., & Oki, S. (2022). ChIP-Atlas 2021 update: a data-mining suite for exploring epigenomic landscapes by fully integrating ChIP-seq, ATAC-seq and Bisulfite-seq data. *Nucleic Acids Research*, *50*(W1), W175-W182. https://doi.org/10.1093/nar/gkac199

Supplemental information

Table S1. Calcium ion homeostasis

	MetaCycle		BioCycle		
Gene	p value	Amplitude	p value	Amplitude	Average TPM[a]
Herp	2.14E-09	11.66	0.00000001	11.35	71.13
Slc4a11	3.22E-09	1.48	0.00000100	1.50	6.68
Sord	3.60E-08	3.60	0.00002116	4.22	42.26
Kcnh1	5.50E-06	0.52	0.00000729	0.40	0.96
Anxa7	6.04E-06	4.44	0.00001444	4.23	102.07
Cx3cl1	3.13E-05	8.76	0.00019881	8.00	80.19
Pik3r1	5.21E-05	2.75	0.00126025	3.17	35.69
Hfe	0.000105052	2.94	0.00001600	2.95	32.10
Nr4a3	0.000106683	2.17	0.00064009	1.94	19.54
Spp1	0.000111664	31.47	0.00978121	41.58	168.53
Nppc	0.000162403	1.71	0.00017424	2.02	11.79
Sumo1	0.000462997	11.16	0.01687401	10.88	128.46
Tns2	0.000494944	1.01	0.00220900	1.21	13.15
Steap3	0.00050386	3.35	0.00494209	2.73	24.42
Capn1	0.000693268	2.57	0.00368449	2.49	48.74
Syt1	0.000707495	0.40	0.00015129	0.29	2.42
Ank	0.000906762	12.09	0.00077284	11.49	220.39
Casq2	0.001722008	0.67	0.00036864	0.64	5.78
Kcnj10	0.003437489	41.65	0.00088804	35.76	485.66
Adora1	0.005727835	6.56	0.00000009	7.08	63.08
P2ry1	0.006372537	1.77	0.00013225	1.99	19.40
Pcgf2	0.020637656	1.69	0.00090601	1.40	31.54
Dgat2	0.032505924	1.49	0.00055225	1.61	15.48

[a]Of all CT-merged values

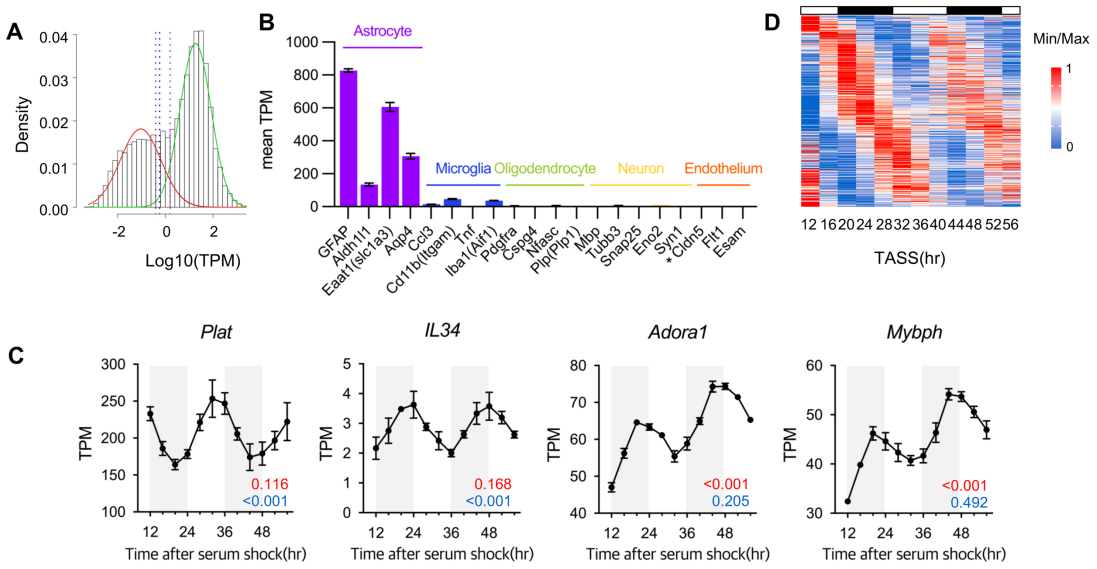

Figure S1. Cluster analysis of astrocyte rhythmic genes. (A) Histogram showing the distribution of mean expression levels of transcripts. Sets of transcripts with low (red) and high (green) expression were defined by modeling the distribution with a Gaussian mixture model. Dashed vertical lines represent the possible cut-off points for defining the set of highly expressed transcripts. Maroon line, 99.5% cut-off point (TPM 0.40); blue line, 99.0% cut-off point (TPM 0.57); purple line, 95.0% cut-off point (TPM 1.59). (B) Time-averaged expression levels of marker genes for astrocytes, microglia, oligodendrocytes, neurons, and endothelial cells in astrocyte cultures. Values are mean TPM ± S.E.M (n = 2); *, not detected in this analysis. (C) Expression profiles of *Plat*, *Il34*, *Adora1*, and *Mybph* in SS-synchronized cultured astrocytes obtained from RNA-seq data. The q-values for BioCycle (red) and MetaCycle (blue) are displayed in the bottom right corner. (D) Heatmap generated by plotting 412 candidate genes obtained from RNA-seq data in ascending order according to their MetaCycle phase. The expression level of each gene was normalized using Min-Max normalization.

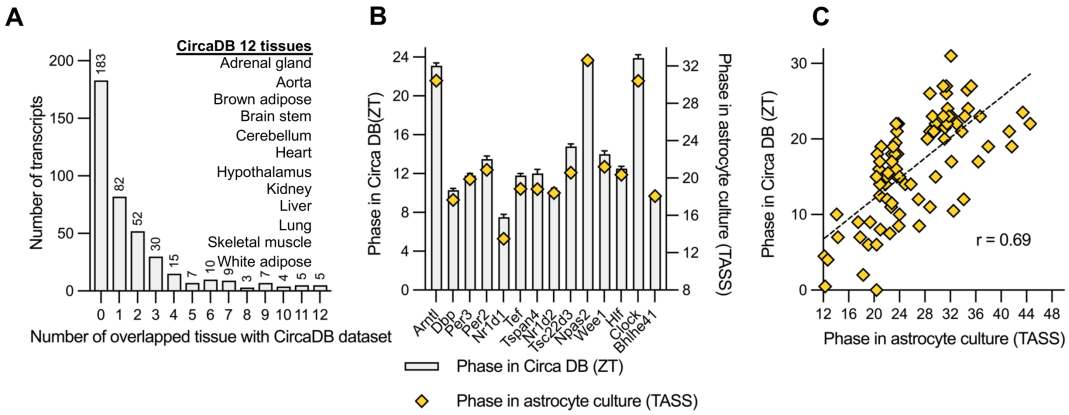

Figure S2. Comparative analysis of circadian rhythmic transcripts in mouse cultured astrocytes and various tissues from CircaDB. (A) Number of transcripts that overlapped with 12 tissues in mouse circadian transcriptome datasets from CircaDB (http://circadb.hogeneschlab.org). (B) Comparison of mean phase (ZT) from CircaDB and phase (TASS) from cultured astrocytes for 14 transcripts that are rhythmic in 10 or more tissues. (C) Scatter plot showing phase in CircaDB and TASS from cultured astrocytes for transcripts that are rhythmic in one tissue.

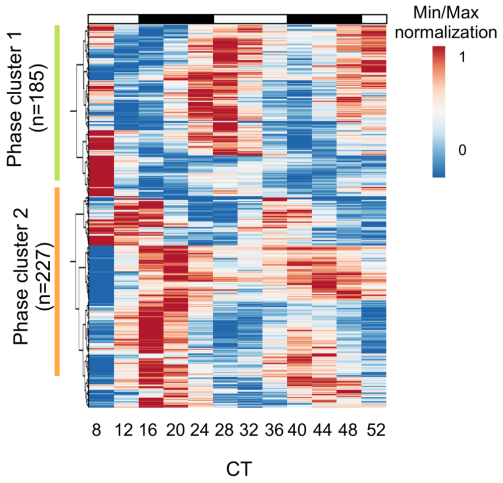

Figure S3. Cluster analysis of astrocyte rhythmic genes. Cluster analysis of 412 candidate genes performed using ClustVis (https://biit.cs.ut.ee/clustvis/)[1]. Expression levels of each gene were normalized using Min-Max normalization. Green bar, Cluster 1; orange bar, Cluster 2.

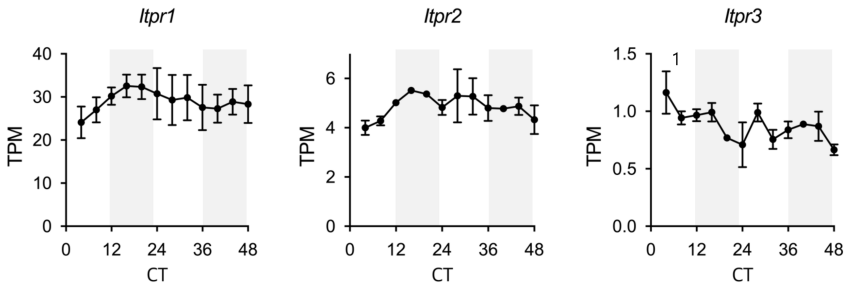

Figure S4. Expression profiles of Itpr1,Itpr2 and Itpr3 in cultured astrocytes obtained from RNA-seq data. White and gray backgrounds represent subjective day and subjective night, respectively.

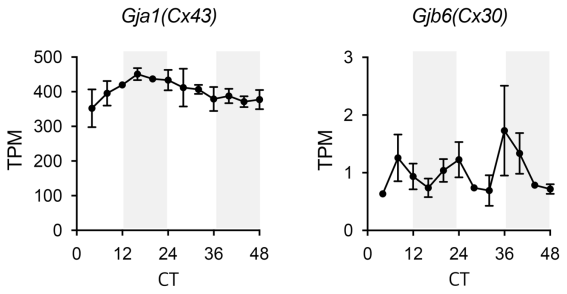

Figure S5. Expression profiles of Cx43 and Cx30 in cultured astrocytes obtained from RNA-seq data. White and gray backgrounds represent subjective day and subjective night, respectively.

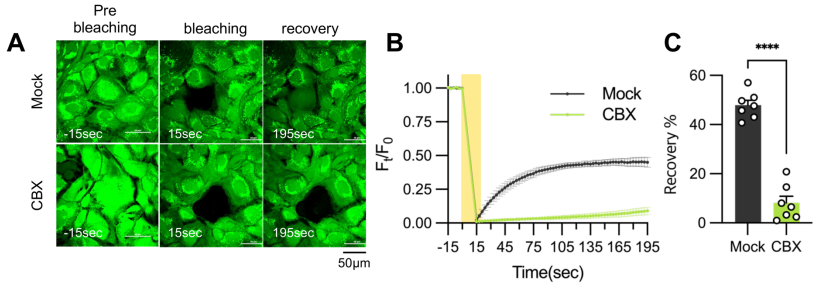

Figure S6. CBX treatment abolished gap junction communication. 20μM carbenoxolone (CBX), a gap junction channel block, was applied to cultured astrocytes for 30 minutes before gap-FRAP analysis. (A) Representative time-lapse images of prebleaching, bleaching and recovery condition during gap-FRAP analysis. (B) Ft/F0 values over time following photobleaching (yellow rectangle). (C) Recovery % values, calculated from panel B. Mock, n = 7; CBX, n = 7. Values in graphs are means ± SEMs (*p < 0.05, **p < 0.005, ***p < 0.0005, and ****p < 0.00005; independent t-test).

SI References

1. Metsalu, T., and Vilo, J. (2015). ClustVis: a web tool for visualizing clustering of multivariate data using Principal Component Analysis and heatmap. Nucleic Acids Res *43*, W566-570. 10.1093/nar/gkv468.